HHS Public Access

Author manuscript

NMR Biomed. Author manuscript; available in PMC 2020 October 01.

Published in final edited form as:

NMR Biomed. 2019 October ; 32(10): e4018. doi:10.1002/nbm.4018.

Probing carbohydrate metabolism using hyperpolarized ^{13}C-labeled molecules

Jaspal Singh[1], **Eul Hyun Suh**[1], **Gaurav Sharma**[1], **Chalermchai Khemtong**[1], **A. Dean Sherry**[1,2], **Zoltan Kovacs**[1]

[1]Advanced Imaging Research Center, The University of Texas Southwestern Medical Center, Dallas, TX, USA

[2]Department of Chemistry and Biochemistry, The University of Texas at Dallas, Richardson, TX, USA

Abstract

Glycolysis is a fundamental metabolic process in all organisms. Anomalies in glucose metabolism are linked to various pathological conditions. In particular, elevated aerobic glycolysis is a characteristic feature of rapidly growing cells. Glycolysis and the closely related pentose phosphate pathway can be monitored in real time by hyperpolarized ^{13}C-labeled metabolic substrates such as ^{13}C-enriched, deuterated D-glucose derivatives, [2-^{13}C]-D-fructose, [2-^{13}C] dihydroxyacetone, [1-^{13}C]-D-glycerate, [1-^{13}C]-D-glucono-δ-lactone and [1-^{13}C] pyruvate in healthy and diseased tissues. Elevated glycolysis in tumors (the Warburg effect) was also successfully imaged using hyperpolarized [U-$^{13}C_6$, U-$^{2}H_7$]-D-glucose, while the size of the preexisting lactate pool can be measured by ^{13}C MRS and/or MRI with hyperpolarized [1-^{13}C]pyruvate. This review summarizes the application of various hyperpolarized ^{13}C-labeled metabolites to the real-time monitoring of glycolysis and related metabolic processes in normal and diseased tissues.

Keywords

dynamic nuclear polarization; glycolysis; hyperpolarized ^{13}C NMR; metabolic probes

1 | INTRODUCTION

Glucose is a fundamental source of energy in living cells. It is present in all living organisms and utilized by both aerobic and anaerobic organisms.[1] In eukaryotes, oxidation of glucose through glycolysis and the citric acid cycle (or tricarboxylic acid cycle, TCA cycle) yields energy in the form of ATP along with the release of carbon dioxide (CO_2) and water. Glycolysis, the breakdown of glucose, includes several reversible and three irreversible (committed) enzymatic reactions leading to the end-product pyruvate (Figure 1).[2,3] The enzymes of the three committed steps in glycolysis are allosterically controlled both

Correspondence: A. Dean Sherry, Advanced Imaging Research Center; 5323 Harry Hines Blvd, Dallas, TX 75390, USA., dean.sherry@utsouthwestern.edu; Zoltan Kovacs, Advanced Imaging Research Center; 5323 Harry Hines Blvd, Dallas, TX, USA. zoltan.kovacs@utsouthwestern.edu.

positively and negatively.[4–8] Pyruvate is a key metabolic intermediate with many potential fates, including the production of carbohydrates through gluconeogenesis, fatty acids, amino acids or energy (ATP) via acetyl-CoA. Anomalies in glucose metabolism are linked to various pathological conditions,[9–11] so any method that could reliably monitor glucose metabolism in vivo not only would be valuable in fundamental studies of those diseases but could also be a valuable diagnostic biomarker. It has been widely documented that tumors and other rapidly proliferating cells have a dramatic increased rate of glucose uptake and lactate production even in the presence of adequate oxygen supply (the Warburg effect).[9,12,13] In addition, the expression levels of the mono-carboxylate transporters MCT1 and MCT4 are higher in cancer, and this facilitates the export of lactate from cancer cells. Although there is still an ongoing debate about why aerobic glycolysis is advantageous for tumor growth, in general cancer cells modulate glucose uptake as well as several glycolytic enzymes to match their energy demands by rapidly, albeit inefficiently, producing ATP in aerobic glycolysis, and to fulfill their increased demand for anabolic intermediates.[14–17] It has also been suggested that acidification of the microenvironment as a result of lactate and acid secretion promotes invasiveness.[18] The tumor suppressor gene *TP53* influences glycolysis at many points to regulate energy metabolism.[19] Intermediate metabolites produced in glycolysis are also used by branching pathways, such as the pentose phosphate pathway (PPP), glycogenesis, hexosamine synthesis pathways and serine biosynthesis to generate nucleotides, amino acids and fatty acids for rapidly proliferating cells. These various pathways are also critically regulated by several oncoproteins and tumor suppressors.[20–22]

This review focuses on the application of hyperpolarized ^{13}C-labeled metabolites for real-time monitoring of glycolysis and related metabolic processes in normal and diseased tissues, with an emphasis on tumor metabolism.

2 | CONVENTIONAL ASSESSMENT OF GLYCOLYSIS

Glycolytic flux is measured as the moles of glucose converted to lactate per unit time, usually normalized per microgram of protein. Glycolytic flux in in vitro cell culture studies is usually determined using a metabolic stress test. The technique is based on measuring the extracellular acidification rate (ECAR) of the surrounding media due to secretion of lactate plus protons after feeding glucose to the cells. Pyruvate produced from glucose can either be converted to lactate, which is then exported to the media along with protons, or it can be oxidized in the TCA cycle to three equivalents of CO_2 (as bicarbonate) and release three H^+ per pyruvate. The acid production due to oxidation can be estimated from the mitochondrial oxygen consumption rate and subtracted from the ECAR. The glycolytic rate is then calculated as the difference between the ECAR before and after addition of glucose minus the acidification due to oxidation. Chemical inhibitors can also be used to separate out other pH effects not associated with lactate production.[23,24] Metabolic flux analyses in cells including flux through single steps of glycolysis have been performed using ^{13}C-labeled glucose derivatives and gas chromatography/mass spectrometry (GC/MS). Fluxes were calculated by fitting the GC/MS data to a model involving all steps in glycolysis, the PPP, the TCA cycle and anaplerotic reactions.[25]

The rate limiting step of glycolysis is debatable, although the phosphofructokinase catalyzed reaction has a complex regulatory mechanism and is generally regarded as the step that determines overall glycolytic flux.[26,27] However, aerobic glycolysis in tumor cells may be limited by glucose uptake.[28] Glucose derivatives labeled with various radioactive isotopes and fluorescent dyes have been used to monitor increased glucose uptake associated with a high glycolytic rate in vivo.[23,29,30] These include 2-deoxy-D-[1,2-^{3}H]-glucose, 2-deoxy-D-[1-^{14}C]-glucose, 2-deoxy-2-(^{18}F)-fluoro-D-glucose (^{18}F-FDG) and the fluorescent probe 2-[N-(7-nitrobenz-2-oxa-1,3-diaxol-4-yl)amino]-2-deoxyglucose (2-NBDG).[31–35] The 2-deoxyglucose derivatives are transported into the cells by glucose transporters and phosphorylated by hexokinases at the C6 position, thereby trapping the tracer inside the cells.[36] However, phosphorylated 2-deoxyglucose derivatives cannot be further metabolized because of the absence of a hydroxyl group at the C2 position, so glycolysis beyond the phosphorylation step cannot be observed.[36,37]

In the clinical setting, positron emission tomography (PET), in particular ^{18}F-fluorodeoxyglucose (^{18}F-FDG), is being extensively used to detect glucose uptake into the cells in vivo.[38–41] In cancer, ^{18}F-FDG can detect changes in metabolic activities well before morphological changes are observed.[42] Thus, ^{18}F-FDG has become an extremely valuable tool in the clinic to diagnose and stage tumors and to monitor cancer treatment (Figure 2).[42–45] However, it should be kept in mind that, unlike MRS, PET cannot distinguish between different molecular species labeled with the same positron emitting isotope. Nevertheless, a specific step in the glycolysis can be probed with a non-FDG-PET-tracer that is designed to bind to the enzyme catalyzing that specific step. For example, the expression of pyruvate kinase M2 (PKM2), an enzyme that catalyzes the final step in glycolysis (Figure 1), has been measured using [^{11}C]DASA-23(1-((2,6-difluorophenyl)sulfon-yl)-4-((4-(methoxy-^{11}C)phenyl)sulfonyl)piperazine) in a preclinical model of glioblastoma multiforme.[46] This tracer binds to the dimeric form of PKM2, which signals increased glycolytic activity in tumors where PKM2 is preferentially expressed. Although PET tracers can be detected in the nanomolar range, the absence of spectral information limits the obtainable biological information compared with MRS.

The crucial role of glucose in various metabolic pathways makes ^{13}C-labeled glucose derivatives and ^{13}C MRS, often in conjugation with mass spectrometry, the obvious choice for monitoring glycolysis in vitro as well as in vivo.[47,48] In an early study, [1-^{13}C]-D-glucose was given to yeast, *Candida utilis*, to follow glucose metabolism by detecting labeled metabolic products.[49] Since then, despite its low sensitivity, ^{13}C MRS has become a useful tool for observing glucose metabolism in vivo, and both direct ^{13}C and indirect ^{13}C-^{1}H MRS have been used for metabolic sudies.[50,51] In vivo MRS facilitates in situ molecular analysis by taking advantage of chemical shift differences between individual atoms in each metabolite. If the concentration of each metabolite of interest is high enough for detection by NMR, then this would allow any metabolic tracer molecule to be observed separately from its downstream metabolic products. The intrinsic low sensitivity of conventional NMR methods is a major disadvantage in that the concentration of many glycolytic intermediates may be below the detection limit of NMR. Proton MRS (^{1}H MRS) can detect lactate with relatively high signal-to-noise ratio and spatial resolution owing to the high receptivity of the ^{1}H nucleus and the relatively high in vivo concentration of lactate

in tumor tissues.[52] However, lactate measurements by ^{1}H MRS can be restricted by overlap of the lactate methyl proton resonance with the highly abundant lipid resonances.[53] This necessitates the use of spectral editing techniques, and accurate quantification also requires water suppression.[54–57] ^{13}C NMR offers higher spectral resolution than ^{1}H NMR due to the larger ^{13}C chemical shift dispersion, but the low sensitivity of the ^{13}C nucleus can impose prohibitively long acquisition times in vivo and ^{13}C-labeled metabolites present at less than 0.1 mM generally cannot be observed.[58] Nevertheless, it was demonstrated that [3-^{13}C] lactate and other metabolites could be detected in tumors by in vivo ^{13}C MRS using a ^{1}H/^{13}C polarization transfer sequence after the intravenous infusion of [1-^{13}C]-D-glucose into a patient with high grade glioma with an acquisition time of about 10 min (Figure 3).[59]

In recent years, however, hyperpolarization of stable isotope-labeled substrates and subsequent magnetic resonance detection has allowed the real-time non-invasive monitoring of glycolysis and other metabolic processes both in vitro and in vivo.[60–64]

3 | HYPERPOLARIZATION

In conventional NMR, the signal intensity is proportional to the difference in the spin population of the Zeeman levels according to the Boltzmann distribution at thermal equilibrium. Unfortunately, the energy difference between the Zeeman levels at or near room temperature and common magnetic field strengths is lower than the ambient thermal energy, and in consequence these levels are almost equally populated. This relative difference in the nuclear spin populations is referred to as nuclear spin polarization (P) and gives rise to the NMR signal. Nuclear spin polarization is a function of applied magnetic field and temperature (proportional to B_0/T) along with a constant known as the magnetogyric ratio (γ), which is nucleus specific. The polarization at thermal equilibrium can be enhanced to some extent by increasing the external magnetic field and/or lowering the temperature, but the effect is not very significant at feasible magnetic fields and temperatures. For example, at 37 °C the ^{13}C spin polarization is about 1.2×10^{-6} and 8.4×10^{-6} at 1.5 T and 7 T, respectively. Nevertheless, moderate liquid state ^{13}C polarizations (about 0.1 %) of [1-^{13}C] pyruvic acid, [1-^{13}C] sodium lactate and [1-^{13}C] acetic acid were achieved with the brute force method of polarization, which only employs high magnetic fields and low temperatures (in this case 14 T and 2.3 K over 10 h).[65]

Much higher signal enhancement can be achieved by raising the nuclear spin polarization above the thermal equilibrium level, a state known as hyperpolarized spin distribution. These non-equilibrium spin populations can be achieved artificially by various experimental methods such as dynamic nuclear polarization (DNP), spin-exchange optical pumping and para-hydrogen induced polarization (PHIP).[66–76] Among these methods, DNP has been extensively used to polarize a wide range of nuclei including ^{13}C, ^{15}N, ^{1}H, ^{31}P, ^{29}Si, ^{19}F, ^{6}Li,^{133}Cs, ^{89}Y and ^{107,109}Ag, and it is currently the preferred technique to polarize ^{13}C-labeled compounds for metabolic studies.[77–89]

DNP is a phenomenon in which the high spin polarization of electrons at low temperatures and high magnetic fields is transferred to coupled nuclei by microwave irradiation at or near the electron spin resonance frequency. The phenomenon was first predicted theoretically by

Overhauser in 1953 and soon thereafter was experimentally demonstrated by Carver and Slichter in solid state.[90–92] Initially, DNP was only used to polarize ^{1}H, ^{13}C or ^{15}N spins in the solid state. In 2003, it was demonstrated in ground-breaking experiments that the compounds hyperpolarized in the solid state could be dissolved and transferred into an NMR magnet for spectrum acquisition with negligible loss of polarization during the transfer process.[93] Experimentally, dissolution DNP-NMR is performed in a glass matrix that involves doping the sample with a stable free radical such as trityl OX063, BDPA or TEMPO, cooling it to around 1 K in a strong magnetic field (3 to 5 T) and irradiating the frozen sample with microwaves near the frequency of the electron spin. The frozen hyperpolarized sample is then rapidly dissolved in a superheated solvent to produce a solution of the hyperpolarized compound at or near room temperature.[87,93] Dissolution DNP polarizers such as HyperSense or SPINlab are available commercially.[94] The dissolution DNP technique has been successfully used to generate hyperpolarized ^{13}C spin systems for molecular MRI applications in vivo.[94–103]

Another method of generating non-equilibrium spin populations relies on the long lived singlet spin state of the para-hydrogen (para-H_2) molecule. PHIP involves the addition of para-H_2 to an unsaturated organic molecule using a catalyst and converting the spin order of the para-H_2 molecule into ^{1}H nuclear polarization.[104,105] After addition to an unsaturated site, the asymmetric proton polarization originating from the para-H_2 can then be transferred to spin-coupled ^{13}C and ^{15}N nuclei by using either RF pulses or magnetic field cycling.[106–108] The applicability of PHIP is limited by the specific chemistry required for the addition of H_2 to unsaturated bonds. Nevertheless, PHIP can be a practical alternative to DNP in some cases. It has been recently adapted to the hyperpolarization of metabolically important carboxylic acids such as acetate and pyruvate by adding para-H_2 to an unsaturated ester followed by the rapid hydrolysis of the ester.[109,110] The main advantages of PHIP over DNP are the rapid generation of hyperpolarized substrates and much less expensive hardware.

It should be emphasized that, regardless of the method used to generate polarization, the hyperpolarized spin state is not persistent and decays to thermodynamic equilibrium by spin-lattice relaxation, a process characterized by the spin-lattice relaxation time, T_1. This limits the detectable NMR signal to about 5 T_1. Therefore, long T_1 values are essential for biomedical imaging with hyperpolarized agents. In general, nuclei with lower γ tend to have longer T_1 values.[13] C nuclei have T_1 relaxation times ranging from a few seconds to about 2 min. The structural position of the ^{13}C label and the molecular weight of the compound largely determine the T_1 relaxation time.[87] Attached protons induce very efficient dipolar relaxation, so replacing them with deuterium, which has a lower γ, can significantly increase the ^{13}C relaxation time.[111] The slowest ^{13}C relaxation rates are observed in functional groups in which the ^{13}C nuclei are not directly bonded to proton (carbonyl, carboxyl and quaternary carbons).[112] The inevitable decay of polarization largely restricts the observable biochemical processes to rapid metabolic pathways that yield metabolites of sufficiently long T_1.[94]

4 | HYPERPOLARIZED ^{13}C PROBES FOR CARBOHYDRATE METABOLISM

^{13}C-labeled glucose derivatives as well as several glycolytic intermediates have been used to monitor glycolysis using hyperpolarized ^{13}C MRS and MRI (Chart 1).

4.1 | ^{13}C-enriched, deuterated D-glucose derivatives

Since glycolysis involves the conversion of glucose to pyruvate, one would anticipate that hyperpolarized ^{13}C-labeled glucose derivatives might be ideal probes to monitor the entire glycolytic pathway in real time with high temporal resolution. However, non-deuterated [1-^{13}C]-D-glucose was found to be unsuitable for metabolic studies on account of its very short T_1 value (<2 s).[112–114] The extremely short T_1 value of glucose can be attributed to the dipole-dipole relaxation of the protonated carbons by ^{1}H spins in the molecule. It is therefore advantageous to replace ^{1}H nuclei (γ_{1H} = 42.6 MHz/T) directly bonded to ^{13}C carbons with ^{2}H spins (γ_{2H} = 6.54 MHz/T).[114] As expected, perdeuterated, uniformly ^{13}C-labeled glucose ([U-$^{13}C_6$, U-$^2H_7$]-D-glucose) has significantly longer T_1 values than the non-deuterated derivative, in the range of about 8 to 15 s, depending on the magnetic field and concentration.[64,112,114] The T_1 values are typically shorter at high magnetic fields and/or in concentrated solutions. D-glucose exists as a mixture of two anomers (α and β-glucopyranose), whose interconversion is slow on the NMR timescale.[115–117] Since these anomers are diastereomers, they have slightly different ^{13}C chemical shifts (Figure 4).[62]

Early attempts to study glycolysis using hyperpolarized glucose derivatives were performed in yeast (*Saccharomyces cerevisiae*) and *Escherichia coli* as model organisms.[60,61] When hyperpolarized [U-$^{13}C_6$, U-$^2H_7$]-D-glucose was used as metabolic substrate for *S. cerevisiae* strain BY4743,[61] ^{13}C NMR spectra indicated the formation of fructose 1,6-bisphosphate, dihydroxyacetone phosphate (DHAcP) and pyruvate as main downstream metabolites resulting from the degradation of glucose (Figure 5). CO_2 and ethanol formed by the decarboxylation of the pyruvate by pyruvate decarboxylase and the reduction of the resultant acetaldehyde by NADH and alcohol dehydrogenase were also observed (Figure 6). The appearance of 6-phosphogluconate reflects the active oxidative phase of the PPP.[61] *E. coli* BL21 cells produced similar glycolytic intermediates but the signal maxima appeared somewhat earlier, suggesting that glycolytic flux is faster in this organism than in *S. cerevisiae* (Figure 6). Intermediates and products detected in *E. coli* included gluconate-6-phosphate, fructose-1,6-bisphosphate, DHAcP, pyruvate, acetyl CoA, lactate, alanine, acetate, formate, CO_2, bicarbonate, ribulose-5P and ethanol. In both organisms, DHAcP, an early downstream product in glycolysis, appeared within a few seconds of infusion, followed by pyruvate and CO_2 shortly after DHAcP. The ^{13}C signal of these intermediates reached maximum intensity within 5 s after glucose infusion indicative of rapid enzymatic reactions. Bicarbonate, acetate or formate reached maxima in approximately 10 s. A signal from ethanol was detected considerably later in both cases.[60] Interestingly, an early paper on the application of ^{13}C NMR for metabolic studies demonstrated that the metabolic rates of the α and β anomers of [1-^{13}C]-D-glucose differ in *E. coli*.[118]

The T_1 value of perdeuterated, ^{13}C-labeled glucose is relatively short, only around 10 s. Thus, for in vivo studies, the hyperpolarized glucose must be dissolved, transferred and injected as fast as possible, preferably in less than 10 s to prevent significant loss of

magnetization. The dissolution and transfer time of the HyperSense commercial polarizer as well as some home-built polarizers is around 8 to 15 s.[63,119] This dead time results in substantial loss of polarization during dissolution and transfer, especially when the T_1 value is comparable to or less than the transfer time. However, technological improvements of the transfer and injection system to shorten the transfer and injection time have been developed.[120,121] Some of these home-built, automated transfer and injection devices reduce the transfer times to about 2 s, and also allow for the neutralization of the free radical polarizing agent and measurement of polarization level inside the imaging magnet.[120] In addition, automated injection systems provide constant flow rate, thereby improving the reproducibility of administration.[94] When hyperpolarized [U-$^{13}C_6$, U-$^{2}H_7$]- D-glucose was administered to healthy mice using the rapid transfer and injection system, it was possible to detect uniformly ^{13}C-labeled lactate in brain at 183.5 ppm 10 s after injection of hyperpolarized glucose (Figure 7).[64] However, the peak appeared as a doublet due to the ^{13}C homo nuclear scalar coupling present in the molecule. The signal to noise of lactate C1 was improved about twofold when [3,4-$^{13}C_2$, 2,3,4,6,6-$^{2}H_5$]-D-glucose was used because the C3-C4 bond is cleaved by aldolase to yield single ^{13}C-enriched C1-labeled molecules in all subsequent three-carbon intermediates including [1-^{13}C] lactate (Figure 7). The ^{13}C nuclei in [3,4-$^{13}C_2$, 2,3,4,6,6-$^{2}H_5$]-D-glucose and [U-$^{13}C_6$, U-$^{2}H_7$]-D-glucose had similar T_1 values, indicating that ^{13}C homonuclear coupling is not a major source of ^{13}C relaxation. Since the Warburg effect is such a characteristic feature of cancer cells, the most interesting application of hyperpolarized glucose is the study of glycolysis in cancer. When hyperpolarized [U-$^{13}C_6$,U-$^{2}H_7$]-D-glucose was injected into a human T47D breast cancer cell suspension, both the C1 and C3 of labeled lactate were observed in the ^{13}C spectra (Figure 8).[62] To preserve the polarization of the glucose carbons, selective shaped pulses were used that applied a low flip angle (1°) to the glucose carbon region (60 to 100 ppm) and a 90° flip angle to the lactate carbonyl (160 to 220 ppm) and methyl regions (20 to 40 ppm).[62] Fitting of the NMR data to a kinetic model revealed that the formation of lactate from glucose followed the Michaelis-Menten kinetics. The peaks that emerged at 212.5 and 179.9 ppm were assigned to the C2 of DHAcP and C1 of 3-phosphoglycerate (3PG), respectively. Other glycolytic intermediates, glucose 6-phosphate, fructose 6-phosphate, fructose 1,6-bisphosphate, glyceraldehyde 3-phosphate (G3P), phosphoenolpyruvate (PEP) and pyruvate, could be observed indirectly by saturation transfer methods.

The metabolism of hyperpolarized [U-$^{13}C_6$, U-$^{2}H_7$]-D-glucose in MCF7 human breast cancer cells and PC3 human prostate cancer cells also produced observable signals of DHAcP (C2, 212.6 ppm), pyruvate (C2, 206.4 ppm, C1, 171.6 ppm) and lactate (C1, 183.5 ppm) as major glycolytic intermediates (Figure 8).[122] Kinetically, the C2 resonance of DHAcP was first to appear, followed by the C1 of pyruvate and lactate, with the maximum signal intensity of C2 DHAcP appearing around 11 s after infusion. The NMR data were fitted to a kinetic model to determine the cytosolic [lactate]/[pyruvate] ratio, and, by calculation, the free [NAD^+]/[NADH] ratio. 6-Phosphogluconate (179.8 ppm) and 6-phosphogluconolactone (177.0 ppm) formed in the PPP also appeared immediately after addition of glucose along with hyperpolarized bicarbonate, formed by the decarboxylation of either pyruvate or 6-phosphogluconate (detected as a singlet at 161.4 ppm, Figure 8). The

peak intensities varied according to the metabolic rate in different tumor cells; for example, the rate of glycolysis in MCF7 cells was found to be about twice as fast as that in PC3 cells.

Hyperpolarized [U-$^{13}C_6$, U-$^{2}H_7$]-D-glucose was successfully used to monitor glycolytic activity by ^{13}C MRS/MRI in tumor bearing animals. When hyperpolarized [U-$^{13}C_6$, U-$^{2}H_7$]-D-glucose was injected into mice with EL4 lymphoma or LL2 Lewis lung carcinoma tumors grown in the lower flank, the C1 carbon of lactate was clearly detected as a doublet using a surface receive coil positioned over the tumor 15 s after injection (the total time between dissolution and data acquisition was about 30 s).[63] Low levels of DHAcP and bicarbonate, as well as a signal around 181 ppm, tentatively assigned to the PPP intermediate 6-phosphogluconate (6-PG), were also observed. ^{13}C chemical shift imaging performed 15 s after injection nicely illustrated the spatial distribution of hyperpolarized glucose and lactate, clearly demonstrating that the lactate signal originated from the tumor region (Figure 9). Strong ^{13}C signals of hyperpolarized [U-$^{13}C_6$, U-$^{2}H_7$]-D-glucose was detected in normal brain, heart, liver and kidney, but glycolytic metabolites were not observed in the healthy tissues. This is likely due to the lower glycolytic activity and perhaps the lower expression of glucose transporters in normal tissues compared with tumors.[28,123] A significant decrease in the lactate/glucose signal ratio (62%) was observed when the experiment was performed 24 h after treatment of the EL4 tumor bearing animals with the chemotherapeutic drug etoposide. Thus, hyperpolarized [U-$^{13}C_6$, U-$^{2}H_7$]-D-glucose can also be used to follow treatment.

It is worth noting that, although the use of deuterated metabolic substrates is expected to induce deuterium isotope effects on the metabolic processes, no such effect was observed with deuterated glucose derivatives.[60,124] This was attributed to the multistep nature of glycolysis as well as to the small contribution of the bond breaking steps to the kinetic control of the enzymatic steps.[60]

4.2 | [2-^{13}C] dihydroxyacetone (DHAc)

DHAcP is a key intermediate in the glycolytic pathway. It is formed along with G3P in one of the critically important steps of glycolysis that involves splitting of the six-carbon fructose 1,6-biphosphate into two three-carbon intermediates. Dihydroxyacetone (DHAc) is rapidly phosphorylated to form DHAcP, which is in reversible exchange with glyceraldehyde-3-phosphate (G3P). The C2 carbon of DHAc has sufficiently long T_1 value (approximately 32 s at 9.4 T) and shows promise for investigating both glycolysis and gluconeogenesis. Recently, hyperpolarized [2-^{13}C] DHAc has been used for the real-time detection of glycolysis and gluconeogenesis in liver and kidney.[125,126] The first metabolite of [2-^{13}C] DHAc that was detected within few seconds of [2-^{13}C] DHAc injection was [2-^{13}C]G3P, which is in rapid equilibrium with DHAcP in the triose phosphate isomerase reaction. Interestingly, when isolated mouse livers were perfused with hyperpolarized [2-^{13}C] DHAc under gluconeogenic (fasted) and glycogenolytic (fed) conditions, metabolic intermediates and end products of both glycolysis and gluconeogenesis were observed. These included [2,5-^{13}C]-D-glucose, [2-^{13}C] glycerol 3-phosphate, [2-^{13}C] PEP, [2-^{13}C] pyruvate, [2-^{13}C] alanine and [2-^{13}C] lactate (Figure 10). The formation of downstream metabolites such as [2-^{13}C] PEP, [2-^{13}C] pyruvate, [2-^{13}C] lactate and [2-^{13}C] alanine under

gluconeogenic conditions indicates simultaneous flux in both directions, because the free energy difference between the G3P, DHAcP and PEP is small, so interconversion of these three-carbon intermediates is not constrained by thermodynamics.[127] Consequently, the ^{13}C label in DHAcP rapidly exchanges into 3PG and PEP under both gluconeogenic and glycogenolytic conditions. [2-^{13}C] DHAc is a promising probe for both glycolysis and gluconeogenesis, but its potential as a metabolic probe in cancer has yet to be explored.

4.3 | [1-^{13}C]pyruvate

Pyruvate is an extremely important metabolite, being at the crossroads of major metabolic pathways. Pyruvate is the end-product of glycolysis and can be used as an energy source or converted to carbohydrates, fatty acids, amino acids or ethanol (in yeast). Pyruvate is rapidly transported across cell membranes by monocarboxylate transporters.[128] In addition, pyruvic acid has very favorable properties for dissolution DNP. Pyruvic acid or sodium pyruvate can easily be polarized to a high degree using standard DNP hardware, and the carbonyl carbons, especially the C1 carbon of pyruvate, have very long T_1 values. Thus, not surprisingly, [1-^{13}C] pyruvate has become the preferred choice as a hyperpolarized ^{13}C probe for metabolic studies.[94,96–98,101,129,130] In normal oxidative tissues the main metabolites observed after the injection of hyperpolarized[1-^{13}C] pyruvate included [^{13}C] bicarbonate, [1-^{13}C] alanine and [1-^{13}C]lactate.[131–138] However, in cancer cells, lactate is produced in significantly higher amounts than in normal tissues as a result of the Warburg effect and consequently, hyperpolarized pyruvate made its greatest impact in tumor diagnosis and grading.[100,101,129,139–143] Hyperpolarized [1-^{13}C] pyruvate was one of the first successful implementations of a hyperpolarized probe for real-time metabolic imaging in tumors, as strongly enhanced signal of the lactate C1 carbon was observed in the tumor region after intravenous infusion.[144] An often confounding aspect of hyperpolarized pyruvate metabolism is whether the appearance of hyperpolarized lactate reflects net conversion of pyruvate to lactate, requiring a stoichiometric amount of NADH for each molecule of lactate produced, or more simply reflects exchange of the “labeled” polarized pyruvate with an existing pool of lactate in the active site of lactate dehydrogenase (LDH). In the latter case, a stoichiometric amount of NADH is not required because the reaction catalyzed by LDH is rapid, so interconversion of pyruvate and lactate can occur in both forward and reverse directions with little net change in either NADH or NAD^+ levels. There is strong evidence for the rapid exchange mechanism, while net conversion of pyruvate to lactate is likely small under most conditions.[145–147] Thus, a large hyperpolarized C1 lactate signal can be detected in tissues having a large preexisting lactate pool without significant production of new lactate (Figure 11). In this case, strictly speaking, pyruvate does not directly probe flux through glycolysis but rather reflects the size of the preexisting lactate pool and the activity of LDH itself. However, one could argue that a large preexisting lactate pool may indeed reflect a hyper-glycolytic state of the tissue, so hyperpolarized ^{13}C-pyruvate can provide valuable insights into glycolysis without actually measuring glycolytic flux. In one example, it has been shown that hyperpolarized [1-^{13}C] lactate level in prostate correlates with cancer development and progression in the TRAMP mouse prostate cancer model.[149] Interestingly, the conversion of [1-^{13}C] pyruvate to [1-^{13}C] alanine could be observed at an earlier, pre-glycolytic stage, in the pre-tumor regions of cancer progression in a Myc oncogene driven liver cancer model.[150]

One of the most promising oncological applications of hyperpolarized pyruvate is assessment of treatment response. Chemotherapeutic drugs can induce metabolic changes in tumors much earlier than the decrease in tumor size can be detected.[151,152] It was demonstrated that reduction of lactate pool size due to treatment can be detected with hyperpolarized pyruvate in tumor bearing animals by ^{13}C spectroscopic imaging.[148,153] ^{13}C MRS/MRI with hyperpolarized pyruvate could be advantageously combined with FDG-PET as the former measures the lactate pool size while the latter technique assesses the first stage (glucose uptake and phosphorylation) of the glycolytic pathway (Figure 12).[129,143] It has been demonstrated that areas of high ^{18}F-FDG uptake and [1-^{13}C] lactate production from hyperpolarized [1-^{13}C] pyruvate did not correlate with each other in a large heterogeneous canine tumor, suggesting that elevated glucose uptake and high lactate production occurs in different tumor regions (Figure 13).[154] There is growing evidence that the assessment of tumor metabolic activity may reflect treatment response more accurately than reduction in tumor size.[152,155–157] However, it should be noted that this is not necessarily a measure of long term survival.

4.4 | Other carbohydrate tracers

D-Fructose is a simple 6-carbon ketose. It is an isomer of glucose with a keto group at C2 rather than an aldehyde carbon at C1. In solution, fructose exists as a mixture of the β-pyranose, β-furanose, α-furanose, α-pyranose and open chain forms (68.23%, 22.35%, 6.24%, 2.67% and 0.50%, respectively).[158–160] The uptake and metabolism of fructose (fructolysis) is markedly different from that of glucose.[161,162] After dietary intake, either by ingesting fructose or digesting sucrose (α-D-glucopyranosyl-(1→2)-β-D-fructofuranoside), fructose is transported into enterocytes by a specific fructose transporter, GLUT5. It is generally accepted that only a small portion of fructose is converted to lactate in the enterocytes, and most of the dietary fructose is released into the portal vein and rapidly taken up by the liver via GLUT2 transporters in an insulin-independent manner.[163] A recent paper, however, suggests that fructose in low doses is largely metabolized into glucose, lactate and glycerate in the small intestine, and the liver is exposed to large amounts of fructose only after high doses of dietary fructose intake.[164] In the liver, fructose is phosphorylated at C1 in hepatocytes by fructokinase, which is mainly expressed in the liver, kidneys and intestines. This enzyme should not be confused with phosphofructokinase, which converts fructose 6-phosphate to fructose 1,6-bisphosphate, an important regulatory step in glycolysis. Fructose can also be phosphorylated at C6 by hexokinases, but hepatic fructokinase has much lower K_m than hexokinase so the majority of fructose is phosphorylated at C1 in the liver. Fructose 1-phosphate is then split into DHAcP and glyceraldehyde by aldolase B and subsequently converted to pyruvate and oxidized in the TCA cycle and/or used as gluconeogenic substrates to produce glucose. It is worth noting that uptake and conversion of fructose into trioses is not regulated by insulin.[165] It has been shown in cancer studies that fructose is preferentially metabolized by the non-oxidative PPP to generate precursors for nucleic acid synthesis.[166] The T_1 value of the quaternary hemiketal C2 carbon of non-deuterated fructose is reasonably long, about 16 s at 11.7 T (14 s at 3 T and about 27 s at 14.1 T), while deuterated fructose has a T_1 of 34 s at 11.7 T.[78] [2-^{13}C] Fructose polarizes well in aqueous solution using the trityl OX063 radical as a polarizing agent under standard DNP conditions.[61,167]

Metabolites detected in yeast (*S. cerevisiae*) after the infusion of hyperpolarized [2-^{13}C] fructose included [2-^{13}C] DHAcP and [2-^{13}C]glucose-6P as well as [5-^{13}C] fructose 1,6-bisphosphate, produced by aldol condensation of DHAcP and [2-^{13}C]G3P.[61] A further demonstration of [2-^{13}C] fructose metabolism was seen in the TRAMP mouse, where the only metabolite observed in prostate tumors 15 s after injection of 80 mM hyperpolarized [2-^{13}C] fructose was [2-^{13}C] fructose 6-phospate, reflective of high hexokinase activity in the tumor.[167]

The recently reported hyperpolarized [1-^{13}C]-D-glycerate is another interesting and potentially useful probe for glycolysis, because glycerate is expected to be transported into cells by monocarboxyate transporters and converted into PEP and triose phosphates.[168] The labeled compound was polarized to a high level using a commercial polarizer and the T_1 of the C1 labeled carbonyl was measured as 59.9 ± 3.0 s at 3 T. The probe was investigated in healthy Wistar rat liver under glycolytic (fed) and gluconeogenic (fasted) conditions. [1-^{13}C] Pyruvate (172.1 ppm) and [1-^{13}C] lactate (185.1 ppm) were the main metabolic products formed from [1-^{13}C]-D-glycerate, and the amounts of products were consistent with the metabolic state of the liver. The [1-^{13}C]lactate/[1-^{13}C] pyruvate ratio was higher in fed animals, consistent with a more highly reduced redox state (Figure 14). [^{13}C] Bicarbonate (161.4 ppm) was also observed, albeit with a poor signal to noise ratio.[168] Other metabolites such as alanine and phosphoglycerates could not be detected because the chemical shift of the C1 carbon of those metabolites overlapped with the intense glycerate signal. Hyperpolarized [1-^{13}C]-D-glycerate has not been tested in tumors at this point.

5 | MONITORING THE PPP

The PPP consists of an irreversible oxidative phase (PPP_{ox}), which generates ribulose 5-phosphate plus CO_2 from glucose 6-phosphate, and a reversible non-oxidative phase (PPP_{non}), which produces ribose 5-phosphate plus other three-, four-, six- and seven-carbon sugars. An important role of the PPP_{ox} phase is to generate reducing equivalents in the form of NADPH to maintain intracellular redox homeostasis.[169] The PPP is elevated in cancer to cover the needs of proliferating cells by generating the high NADPH levels required for either de novo lipogenesis or fatty acid synthesis and by producing ribose for the increased nucleic acid synthesis.[22,170]

5.1 | Other metabolites derived from [U-$^{13}C_6$, U-$^{2}H_7$]-D-glucose

A doublet resonance with low signal-to-noise ratio can be observed at around 181 ppm in ^{13}C NMR spectra in yeast, cancer cells and tumor bearing animals after exposure to hyperpolarized [U-$^{13}C_6$, U-$^{2}H_7$]-D-glucose.[61–63] This resonance could potentially originate from the C1 carbon of phosphorylated glycerates, 1,3-bisphosphoglycerate (1,3-PG), 3-phophospglycerate (3-PG) and 2-phosphoglycerate (2-PG) produced in glycolysis or from the C6 carbon of uniformly labeled 6-phosphogluconate (6PG), which is the second intermediate in the PPP. The difference in the ^{13}C chemical shifts of the C1 resonance in 3PG and 6PG is only 0.6 ppm, which makes it difficult to resolve them in vivo. This peak has been assigned to 6PG in mice with EL4 tumors and to 3PG in yeast or breast cancer cells.[61–63] Recently, the ^{13}C-labeled and total concentrations of 6PG in tumor samples from

animals bearing EL4 tumors, as well as in wild type and glucose-6-phosphate dehydrogenase deficient yeast was measured by LCMS/MS after infusion with [U-$^{13}C_6$, U-$^{2}H_7$]-D-glucose.[171] Since about twice as much labeled 6PG as 2PG/3PG was found in the tumor samples, it was concluded that the resonance at about 181 ppm is largely due to the PPP intermediate 6PG in EL4 tumors. This is not surprising because PPP flux is known to be often up-regulated in cancer.[170] However, in both wild type and the glucose-6-phosphate dehydrogenase deficient yeast strains, a cell not capable of producing 6PG, a similar resonance was observed in spectra of cells exposed to hyperpolarized [U-$^{13}C_6$, U-$^{2}H_7$]-D-glucose so in this case, the resonance likely reflects 3PG.

When hyperpolarized [U-$^{13}C_6$, U-$^{2}H_7$]-D-glucose was injected into normal, non-tumor-bearing mice, a weak, broad signal at 180 ppm was also detected in the brain in addition to the C1 lactate signal.[64] Again, this signal could potentially be due to either the C1 of 3PG produced in glycolysis or the C1 of 6-phosphogluconate formed in the PPP, because uniformly ^{13}C-labeled glucose produces fully labeled metabolites. However, a similar resonance also appeared in spectra when the 3,4-$^{13}C_2$-labeled glucose derivative, [3,4-$^{13}C_2$, 2,3,4,6,6-^{2} H_5]-D-glucose, was used in place of the uniformly ^{13}C-labeled glucose. Since C1-labeled gluconolactone cannot form from [3,4-$^{13}C_2$]-D-glucose, this peak could be unambiguously assigned to the C1 of 3PG. Thus, the use of specifically ^{13}C-labeled glucose derivatives can help distinguish between confounding metabolic pathways such as glycolysis and the PPP.

5.2 | [1-^{13}C]-D-glucono-δ-lactone

The conversion of glucose-6-phosphate to 6-phosphogluconolactone by glucose-6-phosphate dehydrogenase (G6PDH) generates NADPH in the first step of PPP, followed by a second reductive step catalyzed by 6-phosphogluconate dehydrogenase to produce ribose-5-phosphate and CO_2. Given that [1-^{13}C]-D-glucono-δ-lactone is reasonably stable, survives dissolution after DNP and is transported into cells by glucose transporters, this molecule was evaluated as probe for the oxidative phase of PPP by detecting the production of hyperpolarized bicarbonate.[172] [1-^{13}C]-D-glucono-δ-lactone was synthesized from [1-^{13}C]-D-glucose under anhydrous conditions as a δ (six-membered ring) lactone. In water, it forms an equilibrium mixture consisting of the five- and six-membered lactones as well as the open chain gluconic acid. However, both the lactone and open chain forms will be metabolized.[173,174] The labeled compound was hyperpolarized under standard DNP conditions and the T_1 values of γ- and δ-[1-^{13}C] gluconolactone were found to be 19.9 and 17.8 s at 9.4 T, respectively. The hyperpolarized compound was evaluated in isolated normal livers and in livers pre-exposed to hydrogen peroxide. The reactive oxygen species, hydrogen peroxide (H_2O_2), is predicted to increase the flux through the oxidative phase of PPP to generate excess NADPH to maintain the cellular redox state.[175] In livers perfused with or without H_2O_2, hyperpolarized bicarbonate was observed a few seconds after the exposure to hyperpolarized [1-^{13}C]-D-glucono-δ-lactone (Figure 15). This shows that the probe is rapidly taken up by the hepatocytes and phosphorylated, and enters the PPP to generate CO_2 and NADPH. In livers perfused with octanoate as the only oxidative energy source, there was no change observed in bicarbonate production after hydrogen peroxide treatment. However, hydrogen peroxide treatment resulted in a twofold increase in hyperpolarized

bicarbonate production in livers perfused with glucose in the presence of insulin. This observation likely reflects the production of sufficient reduction equivalents from octanoate via the β-oxidation pathway to sustain the cellular redox state without elevating flux through PPP_{ox}. These experiments demonstrate that hyperpolarized [1-^{13}C]-D-glucono-δ-lactone is a promising probe of the PPP. This probe has not been evaluated in vivo.

Hyperpolarized [1-^{13}C] dehydroascorbic acid (DHA) could potentially be used to indirectly measure flux through PPP, as the rate of hyperpolarized [1-^{13}C] DHA reduction was found to be elevated in tumors with depleted glutathione pool. This was accompanied by an increase in PPP flux and glutaredoxin activity.[176] Glutaredoxins are a family of redox enzymes that catalyze the glutathione-dependent reduction of dehydroascorbate to ascorbate. Unfortunately, DHA induced transient respiratory arrest, which may limit its in vivo applicability.[176]

6 | CLINICAL TRANSLATION OF HYPERPOLARIZED ^{13}C MRI FOR IMAGING GLYCOLYSIS

Clinical assessment of metabolic activities is increasingly being used in the clinic to arrive at diagnosis and make therapeutic decisions in several disorders, including cancer, diabetes and heart disease.[136,177–181] Apart from the risk associated with radiation exposure to patients, a major disadvantage of PET in comparison with MR methods is that the real-time metabolic imaging of specific enzyme-catalyzed reactions cannot be easily performed with PET tracers, because PET cannot distinguish between different molecular species. The potential to monitor metabolism in real time by measuring flux through specific enzyme steps would be extremely useful clinically to evaluate the extent of heart diseases, the aggressiveness of a tumor or the source of excess glucose production in a diabetic patients. Hyperpolarized ^{13}C MRS/MRI is well suited for this purpose, and the technology is currently being translated into clinical practice.

So far, there have been only a few reports of hyperpolarized ^{13}C MRI of in human patients using [1-^{13}C]pyruvate.[136,182–185] Nelson et al. reported the first human imaging evaluations of hyperpolarized [1-^{13}C] pyruvate in 31 prostate cancer patients.[183] In addition to demonstrating the feasibility of administering and imaging ^{13}C-pyruvate in humans, this study demonstrated that the conversion of hyperpolarized ^{13}C-pyruvate to ^{13}C-lactate was detectable in human prostate tumors. As cautioned earlier, the appearance of hyperpolarized ^{13}C-lactate from hyperpolarized ^{13}C-pyruvate does not directly measure aerobic glycolysis in these tumors, but the ^{13}C-lactate signal in tumors more likely reflects the size of the pre-existing lactate pool in tissues, which may indirectly reflect total glycolytic or LDH activity in the tissues. Therefore, the appearance of hyperpolarized ^{13}C-lactate from hyperpolarized ^{13}C-pyruvate could potentially be used as an indirect index for tissue glycolysis in tumors. Using the ^{13}C-lactate/^{13}C-pyruvate ratios, it has been shown that elevated ratios correlated well with abnormal prostate lesions compared with the normal prostate tissues (Figure 16). The authors suggested that ^{13}C-lactate/^{13}C-pyruvate ratios may be used as a marker for detecting tumors and staging the disease. In a follow-up report, a longitudinal study in a prostate cancer patient with Gleason 4+5 adenocarcinoma and an elevated serum prostate-

specific antigen (PSA) level showed that the appearance of hyperpolarized [1-^{13}C] lactate can be used as an imaging marker to evaluate therapeutic response following androgen deprivation therapy (ADT).[182] In this patient, baseline ^{13}C MRSI detected a large hyperpolarized [1-^{13}C] lactate signal in the tumor prior to treatment but no detectable [1-^{13}C] lactate signal after 6 weeks of ADT. This result shows that preexisting lactate pool (and perhaps total glycolytic activity) decreased following ADT therapy. The tumor size remained relatively unchanged as shown by T_2-weighted MRI, but serum PSA levels dropped after therapy. Despite the small number of subjects, this study demonstrates an important aspect of hyperpolarized ^{13}C magnetic resonance spectroscopy imaging (MRSI) in that tumors of the same types and similar sizes but with different metabolic activities can be differentiated. This result suggests that hyperpolarized ^{13}C MRSI could one day be routinely used to distinguish aggressive from indolent prostate tumors in a single study, thereby greatly benefiting the diagnosis, therapy and management of prostate cancer. Recently, Park et al. demonstrated the feasibility of metabolic imaging in the human brain by hyperpolarized ^{13}C MRI.[184] In this initial study, the metabolism of hyperpolarized [1-^{13}C] pyruvate was imaged in patients with pre-diagnosed brain tumors (Figure 16). Both ^{13}C-lactate and ^{13}C-bicarbonate were detected in the brain, alleviating the concerns about potential transport issues of hyperpolarized [1-^{13}C] pyruvate past the tightly regulated blood-brain barrier. A relatively large [1-^{13}C] lactate signal was observed in this energy-demanding organ as shown by both ^{13}C spectroscopy and ^{13}C MRI of the brain. Interestingly, hyperpolarized ^{13}C-lactate signals are present in both healthy brain tissues and the tumor regions, perhaps because the patients had undergone therapy before the hyperpolarized ^{13}C MRI studies. Nonetheless, the appearance of hyperpolarized ^{13}C-lactate in the brain demonstrates that glycolysis is active in the brain and that imaging conversion of glucose to pyruvate or a three-carbon intermediate to pyruvate may be extremely valuable in identifying the origin of altered metabolism in many types of human brain disease. In another recent study, Miloushev et al. investigated the appearance of hyperpolarized [1-^{13}C] lactate from hyperpolarized [1-^{13}C] pyruvate in brain tumors of four patients.[185] In this study, both dynamic ^{13}C MRS and metabolic maps of [1-^{13}C] lactate were acquired in human brains with untreated, partly treated or recurrent tumors. High hyperpolarized [1-^{13}C] lactate was observed in a patient with an untreated tumor. Surprisingly, this same tumor region showed a hypo-intense signal of ^{18}F-FDG compared with the normal brain tissue in a PET image. Hyperpolarized [1-^{13}C] lactate signals were visible in the tumor regions of two patients with recurrent glioblastoma and anaplastic oligodendroglioma as confirmed by anatomical ^{1}H MRI. However, the [1-^{13}C] lactate signal intensities in the tumor areas were indistinguishable from those of the normal brain within the same subjects. Last but not least, low [1-^{13}C] lactate signals were observed in the tumor of a patient with metastatic ovarian cancer compared with the rest of the brain. The discrepancy in hyperpolarized [1-^{13}C] lactate appearance in different types of brain tumor highlights the complexity of using hyperpolarized ^{13}C MRI to measure the tissue glycolysis in this disease.

In a study not related to cancer, Cunningham and co-workers reported imaging of hyperpolarized [1-^{13}C] pyruvate in hearts of healthy volunteers.[136] The results showed that hyperpolarized ^{13}C-bicarbonate and hyperpolarized-[1-^{13}C] lactate can be imaged with good spatial resolution (Figure 16). In this study, the authors also suggested that the

hyperpolarized ^{13}C-lactate signal may reflect pre-existing lactate in the heart. Perhaps the most interesting result from this study is the ^{13}C-bicarbonate map of the left ventricle, demonstrating that metabolic flux through pyruvate dehydrogenase (PDH) can be imaged in the human myocardium. Although PDH flux does not provide direct information about glycolysis, the activity of the PDH enzyme is highly dependent on nutritional state and cardiovascular diseases.[186,187] This ground-breaking study opens new opportunities to establish accurate imaging tools for the detection and assessment of cardiovascular abnormalities.

7 | LIMITATIONS OF CURRENT TECHNOLOGY

In addition to pyruvate, there are several other, promising hyperpolarized ^{13}C probes for metabolic imaging, but these have yet to be evaluated in patients.[139] For example, hyperpolarized ^{13}C-glucose may be the ideal probe for measuring flux through the glycolytic pathway and for detecting glycolytic intermediates. However, the short T_1 of ^{13}C-glucose and its derivatives remains a major limitation in translating these probes to clinical medicine. Meanwhile, newer probes with longer T_1 values, such as hyperpolarized [2-^{13}C] DHAc, [1-^{13}C]-D-glycerate and [1-^{13}C]-D-glucono-δ-lactone, have not undergone the required optimizations and safety evaluations for use in humans yet.

The SPINlab commercial clinical polarizer was developed and optimized to polarize [^{13}C] pyruvic acid for clinical applications.[188] It has an automated control subsystem for sample analysis (quality control (QC) module) and a sterile, disposable fluid path that contains all the necessary components (sample vial, co-axial tube, dissolution syringe, receiver vessel with QC appendages, 0.2 μm sterile assurance filter and administration syringe) required for DNP, dissolution and subsequent QC.[188] The process uses a trityl free radical polarizing agent (electron paramagnetic agent) that precipitates in the dissolution liquid containing pyruvic acid at pH values below 4.0, and it is removed with an in-line filter.[188] The acid solution is collected in the receiver, where it is mixed with the neutralization medium. The receiver has a QC appendage that measures the ^{13}C polarization, pH, residual free radical concentration, temperature, volume and pyruvate concentration. The neutralized solution is then transferred into a syringe and administered to a patient only after the sample has passed all QC tests.[184,188] The time required for the automatic dissolution and quality assurance process is around 50 to 60 s. While this design works well for hyperpolarized pyruvate, it is inadequate for the dissolution and transfer of other substrates such as ^{13}C-labeled glucose derivatives. Therefore, the dissolution, removal of the radical and subsequent quality assurance must be significantly accelerated to prevent significant loss of polarization.

For human applications, the free radical polarizing agent must be removed from the hyperpolarized solutions before injection. As discussed, SPINlab currently uses a trityl radical that is insoluble in water at pH values below 4.0. Again, this works for pyruvic acid DNP but it would be unsuitable for neutral substrates. However, trityl radicals can also be removed by reversed phase silica sorbent.[188] Other potential alternatives include easily removable heterogeneous polarizing agents such as mesoporous silica with homogeneously dispersed radicals,[189,190] BDPA-doped polystyrene beads[191] or thermo-responsive, spin-labeled hydrogels.[192] Another potential option is the in situ generation of free radicals by

UV irradiation of the substrate itself, which altogether eliminates the need of using any potentially toxic polarizing agents.[193] It was demonstrated that photo-induced radicals can be generated in high enough concentration for DNP by UV irradiation (at 365 nm) of [1-^{13}C] pyruvic acid at 77 K. Upon dissolution, the recombination of the radicals yielded the non-toxic byproducts $^{13}CO_2$ and acetic acid.[193] However, it remains to be seen if this approach can be used for substrates other than pyruvate.

One of the greatest limitations of current dissolution DNP technology as it is employed in commercially available polarizers is the batchwise design and inability to remove polarized samples from the polarizer for storage and use at a later time. The liquid state T_1 relaxation time of ^{13}C is largely determined by the molecular size and structure, magnetic field, temperature, solvent and presence of paramagnetic species.[78,94] As discussed earlier, the T_1 can be prolonged somewhat by deuteration, which eliminates the strong dipolar relaxation effect of ^{1}H nuclei. Nevertheless, ^{13}C T_1 values are generally less than 2 min even for deuterated compounds,[78,194] and it is unreasonable to expect that hyperpolarized magnetization in the liquid state could be preserved for extended periods of time (several hours) to allow for extensive purification or transport. On the other hand, the solid state T_1 values at cryogenic temperatures are several orders of magnitude longer than the liquid state relaxation times.[195] Interestingly, deuteration appears to have a T_1 shortening effect in the solid state in the presence of the free radical.[196] Unfortunately, these long solid state T_1 values cannot be used to preserve the polarization because conventional DNP samples prepared as frozen solutions containing the substrate, polarizing free radicals and glassing agents cannot be extracted from the polarizer as frozen polarized samples without dramatic shortening of the ^{13}C T_1 in the frozen mixture at low field, apparently due to the presence of the free radical.[197] Attempts have been made to overcome this problem by taking advantage of the rapid recombination of the photo-induced radicals occurring above 190 K in pyruvic acid.[198] Warming the DNP sample above this temperature but keeping it below its melting point (285 K) resulted in the complete annihilation of the radicals without significant decay of the ^{13}C polarization. The hyperpolarized, frozen pyruvic acid sample could then be removed from the polarizer and dissolved into an injectable solution several hours later.[198] Another interesting experimental approach for the production of transportable polarized substrates uses TEMPOL (4-hydroxy-2,2,6,6-tetramethylpiperidin-1-oxyl) benzoate dissolved in toluene as polarizing solution.[197] ^{13}C-labeled substrates were ground into a micro-particulate powder and impregnated with the polarizing solution followed by DNP of proton spins and ^{1}H-^{13}C cross polarization at 1.2 K and 6.7 T. The main advantage of this approach is that the polarizing agent is physically separated from the substrate, thereby creating a “trapped” hyperpolarized ^{13}C state. This allowed the transfer of hyperpolarized micro-powder out of the polarizer and storage in liquid helium for later dissolution. Hyperpolarized samples stored at 4.2 K and 1 T for 16 hours showed significant decay of ^{13}C polarization over the storage period (around 1 to 2% ^{13}C polarization remaining) but this could be ameliorated somewhat by storage at higher magnetic field (at 6.7 T the polarization loss in sodium [1-^{13}C] pyruvate was only about 40% over 16 h).[197]

While the liquid state ^{13}C T_1 relaxation times cannot be extended beyond a couple of minutes, long lived singlet spin states offer an intriguing possibility to store the liquid state polarization for longer periods.[199–205] The lifetime for the singlet configuration of strongly

coupled ½ spins in a molecule can be significantly longer, often by an order of magnitude, than the T_1 relaxation time because it is not affected by intra-pair dipole-dipole relaxation.[201–204] Para-hydrogen is a classic example of an extremely long lived singlet state. The coupled spins must be magnetically equivalent, as in para-hydrogen (disconnected eigenstate), or nearly equivalent, as are the ^{13}C spins in [1,2-$^{13}C_2$] pyruvate in earth's magnetic field (pseudo-eigenstate).[201,204] Longitudinal magnetization can be converted into a singlet spin state with specific pulse sequences or by low field manipulations using a mu-shield.[201,204,206] Singlet spin states are NMR silent, but the NMR signal can be detected by allowing the spins to freely evolve in a high magnetic field for pseudo-eigenstate systems or by breaking the symmetry by a chemical reaction.[204] At this point, however, this approach is still in the early developmental stage for in vivo applications, and it is not practical for routine metabolic imaging.[201]

For successful in vivo imaging, rapid delivery of the hyperpolarized substrate to the target site is necessary. This is normally not a problem for well perfused organs, with the important exception of the brain, where transport across the blood-brain barrier can restrict delivery. Preferential uptake of hyperpolarized ethyl [l-^{13}C]-pyruvate in brain compared with pyruvate has been demonstrated,[207] and the use of ester derivatives was suggested as a general strategy to facilitate rapid transport across the blood-brain barrier.[207] It is worth noting that esterification may also enable cellular uptake of di- and poly-carboxylic acids such as succinate that are not transported by monocarboxylate transporters.[208]

8 | CONCLUSION

In conclusion, a collection of recent literature over the past decade has demonstrated the feasibility of characterizing tissue glycolysis with hyperpolarized ^{13}C MR. Despite several reports of hyperpolarized ^{13}C probes that show promise for imaging glycolysis in vivo, pyruvate is the only probe that has been successfully tested in humans. The other ^{13}C-enriched glycolytic intermediates and substrates have not been evaluated in patients yet. As discussed previously, the five pioneering clinical studies of hyperpolarized ^{13}C MRI mainly focused on the practicality of translating this technology to the clinic.[136,182–185] Polarization and delivery of human-dose quantities of hyperpolarized-[1-^{13}C] pyruvate were optimized and any potential acute adverse effects were monitored in patients after the administration of hyperpolarized [1-^{13}C] pyruvate followed by ^{13}C MRI acquisitions. The fate and tissue distribution of the hyperpolarized ^{13}C-metabolites derived from pyruvate were studied and mapped by ^{13}C-specific imaging sequences. However, a direct readout of glycolysis in tissues of interest, i.e. prostate tumors and viable myocardium, has not been established. This is mainly because pyruvate is the end-product of glycolysis and therefore cannot be used to probe specific steps in the glycolytic pathway. Nonetheless, the human studies with hyperpolarized pyruvate have demonstrated that it is possible to safely translate this hyperpolarization technology to patients. It seems inevitable that metabolic imaging with hyperpolarized pyruvate will be applied to other malignancies such as breast cancer and liver cancer as well as to cardiac, renal and hepatic metabolic abnormalities, because this could be done without major changes in the current technology. The clinical translation of other hyperpolarized ^{13}C probes suitable for probing flux through specific steps of glycolysis would require the redesign of the SPINlab clinical polarizer to accommodate agents with

shorter T_1 values. Hopefully, some of these agents, such as hyperpolarized glucose, fructose or dihydroxyacetone, will be evaluated in humans over the next few years, allowing the real-time imaging of this important pathway in many metabolic diseases.

ACKNOWLEDGEMENTS

Financial support from the National Institutes of Health (R37-HL034557 and P41-EB015908) during the writing of this review is gratefully acknowledged.

Funding information

National Institutes of Health, Grant/Award Numbers: EB015908 and HL-034557

Abbreviations:

2PG	2-phosphoglycerate
3PG	3-phosphoglycerate
ADT	androgen deprivation therapy
DHA	dehydroascorbic acid
DHAcP	dihydroxyacetone phosphate
DNP	dynamic nuclear polarization
ECAR	extracellular acidification rate
G3P	glyceraldehyde 3-phosphate
GC/MS	gas chromatography/mass spectrometry
GLUT	glucose transporter
LDH	lactate dehydrogenase
MCT	monocarboxylate transporter
MRSI	magnetic resonance spectroscopy imaging
PDH	pyruvate dehydrogenase
PEP	phosphoenolpyruvate
PET	positron emission tomography
PHIP	para-hydrogen induced polarization
PKM2	pyruvate kinase M2
PPP	pentose phosphate pathway
PSA	prostate-specific antigen
QC	quality control

TCA	tricarboxylic acid

REFERENCES

1. Fothergill-Gilmore LA, Michels PAM. Evolution of glycolysis. Prog Biophys Mol. 1993;59:105–235.
2. Han HS, Kang G, Kim JS, Choi BH, Koo SH. Regulation of glucose metabolism from a liver-centric perspective. Exp Mol Med. 2016;48:e218. [PubMed: 26964834]
3. Schurr A. Lactate, not pyruvate, is the end product of glucose metabolism via glycolysis In: Caliskan M, Kavakli IH, Oz GC, eds. Carbohydrate. Rijeka, Croatia: InTech; 2017:21–35.
4. Schoeneberg T, Kloos M, Brueser A, Kirchberger J, Straeter N. Structure and allosteric regulation of eukaryotic 6-phosphofructokinases. Biol Chem.2013;394:977–993. [PubMed: 23729568]
5. Romeo T, Snoep JL. Glycolysis and flux control. EcoSal Plus. 2014;542:1–22.
6. Aleshin AE, Zeng C, Bourenkov GP, Bartunik HD, Fromm HJ, Honzatko RB. The mechanism of regulation of hexokinase: new insights from the crystal structure of recombinant human brain hexokinase complexed with glucose and glucose-6-phosphate. Structure. 1998;6:39–50. [PubMed: 9493266]
7. Jurica MS, Mesecar A, Heath PJ, Shi W, Nowak T, Stoddard BL. The allosteric regulation of pyruvate kinase by fructose-1,6-bisphosphate. Structure.1998;6:195–210. [PubMed: 9519410]
8. Kemp RG, Foe LG. Allosteric regulatory properties of muscle phosphofructokinase. Mol Cell Biochem. 1983;57:147–154. [PubMed: 6228716]
9. DeBerardinis RJ, Lum JJ, Hatzivassiliou G, Thompson CB. The biology of cancer: metabolic reprogramming fuels cell growth and proliferation. Cell Metab. 2008;7:11–20. [PubMed: 18177721]
10. Anselmino M, Wallander M, Norhammar A, Mellbin L, Rydén L. Implications of abnormal glucose metabolism in patients with coronary artery disease. Diab Vasc Dis Res. 2008;5:285–290. [PubMed: 18958838]
11. Banerjee K, Munshi S, Frank DE, Gibson GE. Abnormal glucose metabolism in Alzheimer's disease: relation to autophagy/mitophagy and therapeutic approaches. Neurochem Res. 2015;40:2557–2569. [PubMed: 26077923]
12. Liberti MV, Locasale JW. The Warburg effect: how does it benefit cancer cells? Trends Biochem Sci. 2016;41:211–218. [PubMed: 26778478]
13. Warburg O, Wind F, Negelein E. The metabolism of tumors in the body. J Gen Physiol. 1927;8:519–530. [PubMed: 19872213]
14. Gatenby RA, Gillies RJ. Why do cancers have high aerobic glycolysis? Nat Rev Cancer. 2004;4:891–899. [PubMed: 15516961]
15. Lunt SY, Vander Heiden MG. Aerobic glycolysis: meeting the metabolic requirements of cell proliferation. Annu Rev Cell Dev Biol. 2011;27:441–464. [PubMed: 21985671]
16. Jose C, Bellance N, Rossignol R. Choosing between glycolysis and oxidative phosphorylation: a tumor's dilemma. Biochim Biophys Acta, Bioenerg. 1807;2011:552–561.
17. Epstein T, Gatenby RA, Brown JS. The Warburg effect as an adaptation of cancer cells to rapid fluctuations in energy demand. PLoS One. 2017;12: e0185085. [PubMed: 28922380]
18. Hay N Reprogramming glucose metabolism in cancer: can it be exploited for cancer therapy? Nat Rev Cancer. 2016;16:635–649. [PubMed: 27634447]
19. Puzio-Kuter AM. The role of p53 in metabolic regulation. Genes Cancer. 2011;2:385–391. [PubMed: 21779507]
20. Tarrado-Castellarnau M, de Atauri P, Cascante M. Oncogenic regulation of tumor metabolic reprogramming. Oncotarget. 2016;7:62726–62753. [PubMed: 28040803]
21. Jones RG, Thompson CB. Tumor suppressors and cell metabolism: a recipe for cancer growth. Genes Dev. 2009;23:537–548. [PubMed: 19270154]
22. Patra KC, Hay N. The pentose phosphate pathway and cancer. Trends Biochem Sci. 2014;39:347–354. [PubMed: 25037503]
23. TeSlaa T, Teitell MA. Chapter Five—Techniques to monitor glycolysis In: Galluzzi L, Kroemer G, eds. Methods in Enzymology. Academic; 2014:91–114.10.1016/B978-0-12-416618-9.00005-4

24. Mookerjee SA, Goncalves RLS, Gerencser AA, Nicholls DG, Brand MD. The contributions of respiration and glycolysis to extracellular acid production. Biochim Biophys Acta, Bioenerg. 2015;1847:171–181.
25. Metallo CM, Walther JL, Stephanopoulos G. Evaluation of ^{13}C isotopic tracers for metabolic flux analysis in mammalian cells. J Biotechnol. 2009;144:167–174. [PubMed: 19622376]
26. Boscá L, Corredor C. Is phosphofructokinase the rate-limiting step of glycolysis? Trends Biochem Sci. 1984;9:372–373.
27. Lenzen S A fresh view of glycolysis and glucokinase regulation: history and current status. J Biol Chem. 2014;289:12189–12194. [PubMed: 24637025]
28. Jiang B Aerobic glycolysis and high level of lactate in cancer metabolism and microenvironment. Genes Dis. 2017;4:25–27. [PubMed: 30258905]
29. Yamamoto N, Ashida H. Evaluation methods for facilitative glucose transport in cells and their applications. Food Sci Technol Res. 2012;18:493–503.
30. Liu T, Zhang J, Wang X, Yang J, Tang Z, Lu J. Radiolabeled glucose derivatives for tumor imaging using SPECT and PET. Curr Med Chem. 2014;21:24–34. [PubMed: 23992343]
31. Jenkins AB, Furler SM, Kraegen EW. 2-Deoxy-D-glucose metabolism in individual tissues of the rat *in vivo*. Int J Biochem. 1986;18:311–318. [PubMed: 3519306]
32. Hansen PA, Gulve EA, Holloszy JO. Suitability of 2-deoxyglucose for *in vitro* measurement of glucose transport activity in skeletal muscle. J Appl Physiol. 1994;76:979–985. [PubMed: 8175614]
33. Neely JR, Denton RM, England PJ, Randle PJ. The effects of increased heart work on the tricarboxylate cycle and its interactions with glycolysis in the perfused rat heart. Biochem J. 1972;128:147–159. [PubMed: 5085551]
34. Mertens K, Mees G, Lambert B, Van de Wiele C, Goethals I. *In vitro* 2-deoxy-2-[^{18}F]fluoro-D-glucose uptake: practical considerations. Cancer Biother Radiopharm. 2012;27:183–188. [PubMed: 22372557]
35. O'Neil RG, Wu L, Mullani N. Uptake of a fluorescent deoxyglucose analog (2-NBDG) in tumor cells. Mol Imaging Biol. 2005;7:388–392. [PubMed: 16284704]
36. Pauwels EKJ, Ribeiro MJ, Stoot JHMB, McCready VR, Bourguignon M, Mazière B. FDG accumulation and tumor biology. Nucl Med Biol. 1998;25:317–322. [PubMed: 9639291]
37. Zhang D, Li J, Wang F, Hu J, Wang S, Sun Y. 2-Deoxy-D-glucose targeting of glucose metabolism in cancer cells as a potential therapy. Cancer Lett. 2014;355:176–183. [PubMed: 25218591]
38. Shukla AK, Kumar U. Positron emission tomography: an overview. J Med Phys. 2006;31:13–21. [PubMed: 21206635]
39. Gambhir SS. Molecular imaging of cancer with positron emission tomography. Nat Rev Cancer. 2002;2:683–693. [PubMed: 12209157]
40. Wood KA, Hoskin PJ, Saunders MI. Positron emission tomography in oncology: a review. Clin Oncol. 2007;19:237–255.
41. Ziegler SI. Positron emission tomography: principles, technology, and recent developments. Nucl Phys A. 2005;752:679–687.
42. Zhu A, Lee D, Shim H. Metabolic PET imaging in cancer detection and therapy response. Semin Oncol. 2011;38:55–69. [PubMed: 21362516]
43. Price P PET as a potential tool for imaging molecular mechanisms of oncology in man. Trends Mol Med. 2001;7:442–446. [PubMed: 11597518]
44. Almuhaideb A, Papathanasiou N, Bomanji J. (^{18}F)-FDG PET/CT imaging in oncology. Ann Saudi Med. 2011;31:3–13. [PubMed: 21245592]
45. Herrmann K, Krause BJ, Bundschuh RA, Dechow T, Schwaiger M. Monitoring response to therapeutic interventions in patients with cancer. Semin Nucl Med. 2009;39:210–232. [PubMed: 19341841]
46. Witney TH, James ML, Shen B, et al. PET imaging of tumor glycolysis downstream of hexokinase through noninvasive measurement of pyruvate kinase M2. Sci Transl Med. 2015;7:310ra169.
47. Bruntz RC, Lane AN, Higashi RM, Fan TWM. Exploring cancer metabolism using stable isotope resolved metabolomics (SIRM). J Biol Chem. 2017;292:11601–11609. [PubMed: 28592486]

48. Lane AN, Fan TWM, Higashi RM. Isotopomer-based metabolomic analysis by NMR and mass spectrometry. Methods Cell Biol. 2008;84:541–588. [PubMed: 17964943]
49. Eakin RT, Morgan LO, Gregg CT, Matwiyoff NA. Carbon-13 nuclear magnetic resonance spectroscopy of living cells and their metabolism of a specifically labeled ^{13}C substrate. FEBS Lett. 1972;28:259–264. [PubMed: 11946872]
50. Gruetter R, Adriany G, Choi IY, Henry PG, Lei H, Oz G. Localized *in vivo* ^{13}C NMR spectroscopy of the brain. NMR Biomed. 2003;16:313–338. [PubMed: 14679498]
51. de Graaf RA, Mason Graeme F, Patel Anant B, Behar Kevin L, Rothman DL. In vivo ^{1}H-[^{13}C]-NMR spectroscopy of cerebral metabolism. NMR Biomed.2003;16:339–357. [PubMed: 14679499]
52. Frahm J, Bruhn H, Gyngell ML, Merboldt KD, Hänicke W, Sauter R. Localized high-resolution proton NMR spectroscopy using stimulated echoes:initial applications to human brain *in vivo*. Magn Reson Med. 1989;9:79–93. [PubMed: 2540396]
53. Wang AM, Leung GKK, Kiang KMY, Chan D, Cao P, Wu EX. Separation and quantification of lactate and lipid at 1.3 ppm by diffusion-weighted magnetic resonance spectroscopy. Magn Reson Med. 2016;77:480–489. [PubMed: 26833380]
54. Schupp DG, Merkle H, Ellermann JM, Ke Y, Garwood M. Localized detection of glioma glycolysis using edited ^{1}H MRS. Magn Reson Med. 1993;30:18–27. [PubMed: 8371670]
55. Mescher M, Merkle H, Kirsch J, Garwood M, Gruetter R. Simultaneous *in vivo* spectral editing and water suppression. NMR Biomed. 1998;11:266–272. [PubMed: 9802468]
56. Star-Lack J, Spielman D, Adalsteinsson E, Kurhanewicz J, Terris DJ, Vigneron DB. *In vivo* lactate editing with simultaneous detection of choline, creatine, NAA, and lipid singlets at 1.5 T using PRESS excitation with applications to the study of brain and head and neck tumors. J Magn Reson. 1998;133:243–254. [PubMed: 9716465]
57. He QH, Shungu DC, Vanzijl PCM, Bhujwalla ZM, Glickson JD. Single-scan in vivo lactate editing with complete lipid and water suppression by selective multiple-quantum-coherence transfer (Sel-MQC) with application to tumors. J Magn Reson B. 1995;106:203–211. [PubMed: 7719620]
58. Henry PG, Deelchand DK, Iltis I, et al. *In vivo*^{13}C magnetic resonance spectroscopy and metabolic modeling: methodology In: Choi IY, Gruetter R, eds. Neural Metabolism In Vivo (Advances in Neurobiology Vol 4) (pp. 181–220). Boston, MA: Springer; 2012.
59. Wijnen JP, Van der Graaf M, Scheenen TWJ, et al. *In vivo* ^{13}C magnetic resonance spectroscopy of a human brain tumor after application of ^{13}C-1-enriched glucose. Magn Reson Imaging. 2010;28:690–697. [PubMed: 20399584]
60. Meier S, Jensen PR, Duus JO. Real-time detection of central carbon metabolism in living *Escherichia coli* and its response to perturbations. FEBS Lett. 2011;585:3133–3138. [PubMed: 21907715]
61. Meier S, Karlsson M, Jensen PR, Lerche MH, Duus JO. Metabolic pathway visualization in living yeast by DNP-NMR. Mol Biosyst. 2011;7:2834–2836. [PubMed: 21720636]
62. Harris T, Degani H, Frydman L. Hyperpolarized ^{13}C NMR studies of glucose metabolism in living breast cancer cell cultures. NMR Biomed. 2013;26:1831–1843. [PubMed: 24115045]
63. Rodrigues TB, Serrao EM, Kennedy BW, Hu DE, Kettunen MI, Brindle KM. Magnetic resonance imaging of tumor glycolysis using hyperpolarized ^{13}Clabeled glucose. Nat Med. 2014;20:93–97. [PubMed: 24317119]
64. Mishkovsky M, Anderson B, Karlsson M, et al. Measuring glucose cerebral metabolism in the healthy mouse using hyperpolarized ^{13}C magnetic resonance. Sci Rep. 2017;7:11719. [PubMed: 28916775]
65. Hirsch ML, Kalechofsky N, Belzer A, Rosay M, Kempf JG. Brute-force hyperpolarization for NMR and MRI. J Am Chem Soc. 2015;137:8428–8434. [PubMed: 26098752]
66. Kuhn LT. Topics in Current Chemistry 338. Hyperpolarization Methods in NMR Spectroscopy. Berlin, Germany: Springer; 2013.
67. Viale A, Aime S. Current concepts on hyperpolarized molecules in MRI. Curr Opin Chem Biol. 2010;14:90–96. [PubMed: 19913452]
68. Canet D, Aroulanda C, Mutzenhardt P, Aime S, Gobetto R, Reineri F. Para-hydrogen enrichment and hyperpolarization. Concepts Magn Reson A. 2006;28A:321–330.

69. Lee JH, Okuno Y, Cavagnero S. Sensitivity enhancement in solution NMR: emerging ideas and new frontiers. J Magn Reson. 2014;241:18–31. [PubMed: 24656077]
70. Nikolaou P, Goodson BM, Chekmenev EY. NMR hyperpolarization techniques for biomedicine. Chemistry. 2015;21:3156–3166. [PubMed: 25470566]
71. Glöggler S, Colell J, Appelt S. Para-hydrogen perspectives in hyperpolarized NMR. J Magn Reson. 2013;235:130–142. [PubMed: 23932399]
72. Iali W, Rayner PJ, Duckett SB. Using parahydrogen to hyperpolarize amines, amides, carboxylic acids, alcohols, phosphates, and carbonates. Sci Adv. 2018;4:eaao6250. [PubMed: 29326984]
73. Siddiqui S, Kadlecek S, Pourfathi M, et al. The use of hyperpolarized carbon-13 magnetic resonance for molecular imaging. Adv Drug Deliv Rev.2017;113:3–23. [PubMed: 27599979]
74. Adams RW, Aguilar JA, Atkinson KD, et al. Reversible interactions with para-hydrogen enhance NMR sensitivity by polarization transfer. Science.2009;323:1708–1711. [PubMed: 19325111]
75. Halse ME. Perspectives for hyperpolarisation in compact NMR. Trends Anal Chem. 2016;83:76–83.
76. Roos JE, McAdams HP, Kaushik SS, Driehuys B. Hyperpolarized gas MR imaging: technique and applications. Magn Reson Imaging Clin N Am. 2015;23:217–229. [PubMed: 25952516]
77. Ardenkjaer-Larsen JH, Johannesson H, Petersson JS, Wolber J. Hyperpolarized molecules in solution. Methods Mol Biol. 2011;771:205–226. [PubMed: 21874480]
78. Keshari KR, Wilson DM. Chemistry and biochemistry of ^{13}C hyperpolarized magnetic resonance using dynamic nuclear polarization. Chem Soc Rev. 2014;43:1627–1659. [PubMed: 24363044]
79. Kockenberger W Dissolution dynamic nuclear polarization. eMagRes. 2014;3:161–170.
80. Guenther UL. Dynamic nuclear hyperpolarization in liquids. Top Curr Chem. 2013;335:23–70. [PubMed: 22025060]
81. Dutta P, Martinez GV, Gillies RJ. A new horizon of DNP technology: application to in-vivo ^{13}C magnetic resonance spectroscopy and imaging. Biophys Rev. 2013;5:271–281. [PubMed: 26491489]
82. Yen Y-F, Nagasawa K, Nakada T. Promising application of dynamic nuclear polarization for *in vivo* ^{13}C MR imaging. Magn Reson Med Sci. 2011;10:211–217. [PubMed: 22214905]
83. van Heeswijk RB, Uffmann K, Comment A, et al. Hyperpolarized lithium-6 as a sensor of nanomolar contrast agents. Magn Reson Med. 2009;61:1489–1493. [PubMed: 19353663]
84. Karlsson M, Ardenkjær-Larsen JH, Lerche MH. Hyperpolarized ^{133}Cs is a sensitive probe for real-time monitoring of biophysical environments. Chem Commun. 2017;53:6625–6628.
85. Lee Y, Zeng H, Ruedisser S, Gossert AD, Hilty C. Nuclear magnetic resonance of hyperpolarized fluorine for characterization of protein-ligand inter-actions. J Am Chem Soc. 2012;134:17448–17451. [PubMed: 23020226]
86. Nardi-Schreiber A, Gamliel A, Harris T, et al. Biochemical phosphates observed using hyperpolarized ^{31}P in physiological aqueous solutions. Nat Commun. 2017;8:341. [PubMed: 28839124]
87. Lumata L, Ratnakar SJ, Jindal A, et al. BDPA: an efficient polarizing agent for fast dissolution dynamic nuclear polarization NMR spectroscopy. Chemistry. 2011;17:10825–10827. [PubMed: 21919088]
88. Lumata L, Jindal AK, Merritt ME, Malloy CR, Sherry AD, Kovacs Z. DNP by thermal mixing under optimized conditions yields >60 000-fold enhancement of ^{89}Y NMR signal. J Am Chem Soc. 2011;133:8673–8680. [PubMed: 21539398]
89. Lumata L, Merritt ME, Hashami Z, Ratnakar SJ, Kovacs Z. Production and NMR characterization of hyperpolarized ^{107,109}Ag complexes. Angew Chem Int Ed. 2011;51:525–527.
90. Overhauser AW. Polarization of nuclei in metals. Phys Ther Rev. 1953;92:411–415.
91. Slichter CP. The discovery and renaissance of dynamic nuclear polarization. Rep Prog Phys. 2014;77:072501. [PubMed: 24994709]
92. Carver TR, Slichter CP. Polarization of nuclear spins in metals. Phys Ther Rev. 1953;92:212–213.
93. Ardenkjaer-Larsen JH, Fridlund B, Gram A, et al. Increase in signal-to-noise ratio of > 10,000 times in liquid-state NMR. Proc Natl Acad Sci U S A. 2003;100:10158–10163. [PubMed: 12930897]

94. Chaumeil MM, Najac C, Ronen SM. Chapter One—Studies of metabolism using 13C MRS of hyperpolarized probes In: Metallo CM, ed. Methods in Enzymology. Academic; 2015:1–71.
95. Månsson S, Johansson E, Magnusson P, et al. ^{13}C imaging—a new diagnostic platform. Eur Radiol. 2006;16:57–67. [PubMed: 16402256]
96. Golman K, Zandt R, Thaning M. Real-time metabolic imaging. Proc Natl Acad Sci U S A. 2006;103:11270–11275. [PubMed: 16837573]
97. Gallagher FA, Kettunen MI, Brindle KM. Biomedical applications of hyperpolarized ^{13}C magnetic resonance imaging. Prog Nucl Magn Reson Spectrosc. 2009;55:285–295.
98. Brindle KM. Imaging metabolism with hyperpolarized ^{13}C-labeled cell substrates. J Am Chem Soc. 2015;137:6418–6427. [PubMed: 25950268]
99. Lumata L, Yang C, Ragavan M, Carpenter N, DeBerardinis RJ, Merritt ME. Chapter Two—Hyperpolarized ^{13}C magnetic resonance and its use in metabolic assessment of cultured cells and perfused organs In: Metallo CM, ed. Methods in Enzymology. Academic; 2015:73–106.
100. Brindle KM, Bohndiek SE, Gallagher FA, Kettunen MI. Tumor imaging using hyperpolarized ^{13}C magnetic resonance spectroscopy. Magn Reson Med.2011;66:505–519. [PubMed: 21661043]
101. Cho A, Lau JYC, Geraghty BJ, Cunningham CH, Keshari KR. Noninvasive interrogation of cancer metabolism with hyperpolarized ^{13}C MRI. J Nucl Med. 2017;58:1201–1206. [PubMed: 28596156]
102. Comment A, Merritt ME. Hyperpolarized magnetic resonance as a sensitive detector of metabolic function. Biochemistry. 2014;53:7333–7357. [PubMed: 25369537]
103. Mishkovsky M, Comment A. Hyperpolarized MRS: new tool to study real-time brain function and metabolism. Anal Biochem. 2017;529:270–277. [PubMed: 27665679]
104. Green RA, Adams RW, Duckett SB, Mewis RE, Williamson DC, Green GGR. The theory and practice of hyperpolarization in magnetic resonance using parahydrogen. Prog Nucl Magn Reson Spectrosc. 2012;67:1–48. [PubMed: 23101588]
105. Hovener J, Pravdivtsev AN, Kidd B, et al. Parahydrogen-based hyperpolarization for biomedicine. Angew Chem Int Ed. 2018 10.1002/ange.201711842
106. Duckett SB, Newell CL, Eisenberg R. More than INEPT: parahydrogen and INEPT+ give unprecedented resonance enhancement to carbon-13 by direct proton polarization transfer. J Am Chem Soc. 1993;115:1156–1157.
107. Reineri F, Viale A, Dastrù W, Gobetto R, Aime S. How to design ^{13}C para-hydrogen-induced polarization experiments for MRI applications. Contrast Media Mol Imaging. 2010;6:77–84. [PubMed: 21504062]
108. Korchak S, Yang S, Mamone S, Glöggler S. Pulsed magnetic resonance to signal-enhance metabolites within seconds by utilizing para-hydrogen.ChemistryOpen. 2018;7:344–348. [PubMed: 29761065]
109. Reineri F, Boi T, Aime S. Parahydrogen induced polarization of ^{13}C carboxylate resonance in acetate and pyruvate. Nat Commun. 2015;6:5858. [PubMed: 25556844]
110. Cavallari E, Carrera C, Boi T, Aime S, Reineri F. Effects of magnetic field cycle on the polarization transfer from parahydrogen to heteronuclei through long-range *J*-couplings. J Phys Chem B. 2015;119:10035–10041. [PubMed: 26161454]
111. Allouche-Arnon H, Lerche MH, Karlsson M, Lenkinski RE, Katz-Brull R. Deuteration of a molecular probe for DNP hyperpolarization—a new approach and validation for choline chloride. Contrast Media Mol Imaging. 2011;6:499–506. [PubMed: 22144028]
112. Kumagai K, Akakabe M, Tsuda M, et al. Observation of glycolytic metabolites in tumor cell lysate by using hyperpolarization of deuterated glucose. Biol Pharm Bull. 2014;37:1416–1421. [PubMed: 25087964]
113. Harada M, Kubo H, Abe T, Maezawa H, Otsuka H. Selection of endogenous ^{13}C substrates for observation of intracellular metabolism using the dynamic nuclear polarization technique. Jpn J Radiol. 2010;28:173–179. [PubMed: 20182855]
114. Allouche-Arnon H, Wade T, Waldner LF, et al. *In vivo* magnetic resonance imaging of glucose—initial experience. Contrast Media Mol Imaging. 2013;8:72–82. [PubMed: 23109395]
115. Gurst JE. NMR and the structure of D-glucose. J Chem Educ. 1991;68:1003–1004.

116. Maple SR, Allerhand A. Detailed tautomeric equilibrium of aqueous D-glucose. Observation of six tautomers by ultrahigh resolution carbon-13 NMR. J Am Chem Soc. 1987;109:3168–3169.
117. Kaufmann M, Mügge C, Kroh LW. NMR analyses of complex D-glucose anomerization. Food Chem. 2018;265:222–226. [PubMed: 29884376]
118. Ugurbil K, Brown TR, Den Hollander JA, Glynn P, Shulman RG. High-resolution carbon-13 nuclear magnetic resonance studies of glucose metabolism in *Escherichia coli*. Proc Natl Acad Sci U S A. 1978;75:3742–3746. [PubMed: 358201]
119. Lumata LL, Martin R, Jindal AK, Kovacs Z, Conradi MS, Merritt ME. Development and performance of a 129-GHz dynamic nuclear polarizer in an ultrawide bore superconducting magnet. Magn Reson Mater Phys Biol Med. 2015;28:195–205.
120. Cheng T, Mishkovsky M, Bastiaansen JAM, et al. Automated transfer and injection of hyperpolarized molecules with polarization measurement prior to *in vivo* NMR. NMR Biomed. 2013;26:1582–1588. [PubMed: 23893539]
121. Reynolds S, Bucur A, Port M, et al. A system for accurate and automated injection of hyperpolarized substrate with minimal dead time and scalable volumes over a large range. J Magn Reson. 2014;239:1–8. [PubMed: 24355621]
122. Christensen CE, Karlsson M, Winther JR, Jensen PR, Lerche MH. Non-invasive in-cell determination of free cytosolic [NAD+]/[NADH] ratios using hyperpolarized glucose show large variations in metabolic phenotypes. J Biol Chem. 2014;289:2344–2352. [PubMed: 24302737]
123. Szablewski L Expression of glucose transporters in cancers. BBA Rev Cancer. 2013;1835;164–169.
124. Funk AM, Anderson BL, Wen X, et al. The rate of lactate production from glucose in hearts is not altered by per-deuteration of glucose. J Magn Reson. 2017;284:86–93. [PubMed: 28972888]
125. Moreno KX, Satapati S, DeBerardinis RJ, Burgess SC, Malloy CR, Merritt ME. Real-time detection of hepaticgluconeogenic and glycogenolytic states using hyperpolarized [2-^{13}C]dihydroxyacetone. J Biol Chem. 2014;289:35859–35867. [PubMed: 25352600]
126. Marco-Rius I, von Morze C, Sriram R, et al. Monitoring acute metabolic changes in the liver and kidneys induced by fructose and glucose using hyperpolarized [2-^{13}C]dihydroxyacetone. Magn Reson Med. 2017;77:65–73. [PubMed: 27859575]
127. Cornish-Bowden A Thermodynamic aspects of glycolysis. Biochem Educ. 1981;9:133–137.
128. Lin R-Y, Vera JC, Chaganti RSK, Golde DW. Human monocarboxylate transporter 2 (MCT2) is a high affinity pyruvate transporter. J Biol Chem. 1998;273:28959–28965. [PubMed: 9786900]
129. Serrao EM, Brindle KM. Potential clinical roles for metabolic imaging with hyperpolarized [1-^{13}C]pyruvate. Front Oncol. 2016;6:59. [PubMed: 27014634]
130. Miloushev VZ, Keshari KR, Holodny AI. Hyperpolarization MRI: preclinical models and potential applications in neuroradiology. Top Magn Reson Imaging. 2016;25:31–37. [PubMed: 26848559]
131. Merritt ME, Harrison C, Sherry AD, Malloy CR, Burgess SC. Flux through hepatic pyruvate carboxylase and phosphoenolpyruvate carboxykinase detected by hyperpolarized ^{13}C magnetic resonance. Proc Natl Acad Sci U S A. 2011;108:19084–19089. [PubMed: 22065779]
132. Merritt ME, Harrison C, Storey C, Jeffrey FM, Sherry AD, Malloy CR. Hyperpolarized ^{13}C allows a direct measure of flux through a single enzyme-catalyzed step by NMR. Proc Natl Acad Sci U S A. 2007;104:19773–19777. [PubMed: 18056642]
133. Jin ES, Moreno KX, Wang J-X, et al. Metabolism of hyperpolarized [1-^{13}C] pyruvate through alternate pathways in rat liver. NMR Biomed. 2016;29:466–474. [PubMed: 26836042]
134. Bhattacharya P, Ross BD, Bünger R. Cardiovascular applications of hyperpolarized contrast media and metabolic tracers. Exp Biol Med. 2009;234:1395–1416.
135. Marjańska M, Iltis I, Shestov AA, et al. *In vivo* ^{13}C spectroscopy in the rat brain using hyperpolarized [1-^{13}C] pyruvate and [2-^{13}C]pyruvate. J Magn Reson. 2010;206:210–218. [PubMed: 20685141]
136. Cunningham CH, Lau JY, Chen AP, et al. Hyperpolarized ^{13}C metabolic MRI of the human heart: initial experience. Circ Res. 2016;119:1177–1182. [PubMed: 27635086]
137. Golman K, Petersson JS, Magnusson P, et al. Cardiac metabolism measured noninvasively by hyperpolarized ^{13}C MRI. Magn Reson Med. 2008;59:1005–1013. [PubMed: 18429038]

138. Mayer D, Yen Y-F, Takahashi A, et al. Dynamic and high-resolution metabolic imaging of hyperpolarized [1-^{13}C]-pyruvate in the rat brain using a high-performance gradient insert. Magn Reson Med. 2010;65:1228–1233. [PubMed: 21500253]

139. Kurhanewicz J, Vigneron DB, Brindle K, et al. Analysis of cancer metabolism by imaging hyperpolarized nuclei: prospects for translation to clinical research. Neoplasia. 2011;13:81–97. [PubMed: 21403835]

140. Viale A, Reineri F, Dastrù W, Aime S. Hyperpolarized ^{13}C-pyruvate magnetic resonance imaging in cancer diagnostics. Expert Opin Med Diagn. 2012;6:335–345. [PubMed: 23480742]

141. Morze C, Merritt ME. Cancer in the crosshairs: targeting cancer metabolism with hyperpolarized carbon-13 MRI technology. NMR Biomed. 2018; e3937. [PubMed: 29870085]

142. Salamanca-Cardona L, Keshari KR. ^{13}C-labeled biochemical probes for the study of cancer metabolism with dynamic nuclear polarization-enhanced magnetic resonance imaging. Cancer Metab. 2015;3:9. [PubMed: 26380082]

143. Gallagher FA, Bohndiek SE, Kettunen MI, Lewis DY, Soloviev D, Brindle KM. Hyperpolarized ^{13}C MRI and PET: *in vivo* tumor biochemistry. J Nucl Med. 2011;52:1333–1336. [PubMed: 21849405]

144. Golman K, Zandt R, Lerche M, Pehrson R, Ardenkjaer-Larsen JH. Metabolic imaging by hyperpolarized ^{13}C magnetic resonance imaging for *in vivo* tumor diagnosis. Cancer Res. 2006;66:10855–10860. [PubMed: 17108122]

145. Witney TH, Kettunen MI, Brindle KM. Kinetic modeling of hyperpolarized ^{13}C label exchange between pyruvate and lactate in tumor cells. J Biol Chem. 2011;286:24572–24580. [PubMed: 21596745]

146. Kettunen MI, Hu D-e, Witney TH, et al. Magnetization transfer measurements of exchange between hyperpolarized [1-^{13}C] pyruvate and [1-^{13}C] lactate in a murine lymphoma. Magn Reson Med. 2010;63:872–880. [PubMed: 20373388]

147. Khemtong C, Carpenter NR, Lumata Lloyd L, et al. Hyperpolarized ^{13}C NMR detects rapid drug-induced changes in cardiac metabolism. Magn Reson Med. 2014;74:312–319. [PubMed: 25168480]

148. Day SE, Kettunen MI, Gallagher FA, et al. Detecting tumor response to treatment using hyperpolarized ^{13}C magnetic resonance imaging and spectroscopy. Nat Med. 2007;13:1382–1387. [PubMed: 17965722]

149. Albers MJ, Bok R, Chen AP, et al. Hyperpolarized ^{13}C lactate, pyruvate, and alanine: noninvasive biomarkers for prostate cancer detection and grading. Cancer Res. 2008;68:8607–8615. [PubMed: 18922937]

150. Hu S, Balakrishnan A, Bok RA, et al. ^{13}C-pyruvate imaging reveals alterations in glycolysis that precede c-Myc-induced tumor formation and regression. Cell Metab. 2011;14:131–142. [PubMed: 21723511]

151. Wieder HA, Beer AJ, Lordick F, et al. Comparison of changes in tumor metabolic activity and tumor size during chemotherapy of adenocarcinomas of the esophagogastric junction. J Nucl Med. 2005;46:2029–2034. [PubMed: 16330567]

152. Van den Abbeele AD. The lessons of GIST—PET and PET/CT: A new paradigm for imaging. Oncologist. 2008;13:8–13. [PubMed: 18434632]

153. Di Gialleonardo V, Aldeborgh HN, Miloushev V, et al. Multinuclear NMR and MRI reveal an early metabolic response to mTOR inhibition in sarcoma.Cancer Res. 2017;77:3113–3120. [PubMed: 28386017]

154. Gutte H, Hansen EA, Larsen MM, et al. *In vivo* phenotyping of tumor metabolism in a canine cancer patient with simultaneous ^{18}F-FDG-PET and hyperpolarized ^{13}C-pyruvate magnetic resonance spectroscopic imaging (hyperPET): mismatch demonstrates that FDG may not always reflect the Warburg effect. Diagnostics. 2015;5:287–289. [PubMed: 26854154]

155. Kim JH, Kim BJ, Jang HJ, Kim HS. Comparison of the RECIST and EORTC PET criteria in the tumor response assessment: a pooled analysis and review.Cancer Chemother Pharmacol. 2017;80:729–735. [PubMed: 28780726]

156. Shady W, Kishore S, Gavane S, et al. Metabolic tumor volume and total lesion glycolysis on FDG-PET/CT can predict overall survival after ^{90}Y radioembolization of colorectal liver

metastases: a comparison with SUVmax, SUVpeak, and RECIST 1.0. Eur J Radiol. 2016;85:1224–1231. [PubMed: 27161074]

157. Birchard KR, Hoang JK, Herndon JE, Patz EF. Early changes in tumor size in patients treated for advanced stage nonsmall cell lung cancer do not correlate with survival. Cancer. 2008;115:581–586.
158. Jaseja M, Perlin Arthur S, Dais P. Two-dimensional NMR spectral study of the tautomeric equilibria of D-fructose and related compounds. Magn Reson Chem. 1990;28:283–289.
159. Barclay T, Ginic-Markovic M, Johnston MR, Cooper P, Petrovsky N. Observation of the *keto* tautomer of D-fructose in D_2O using ^1H NMR spectroscopy. Carbohydr Res. 2012;347:136–141. [PubMed: 22129837]
160. Mega TL, Cortes S, Van Etten RL. The oxygen-18 isotope shift in carbon-13 nuclear magnetic resonance spectroscopy. 13. Oxygen exchange at the anomeric carbon of D-glucose, D-mannose, and D-fructose. J Org Chem. 1990;55:522–528.
161. Sun SZ, Empie MW. Fructose metabolism in humans—what isotopic tracer studies tell us. Nutr Metab. 2012;9:89.
162. Tappy L, Lê K-A. Metabolic effects of fructose and the worldwide increase in obesity. Physiol Rev. 2010;90:23–46. [PubMed: 20086073]
163. Jegatheesan P, De Bandt JP. Fructose and NAFLD: the multifaceted aspects of fructose metabolism. Nutrients. 2017;9:E230. [PubMed: 28273805]
164. Jang C, Hui S, Lu W, et al. The small intestine converts dietary fructose into glucose and organic acids. Cell Metab. 2018;27:351–361. e3 [PubMed: 29414685]
165. Fryburg DA, Gelfand RA. Is exogenous fructose metabolism truly insulin independent? J Parenter Enteral Nutr. 1990;14:535–537.
166. Liu H, Huang D, McArthur DL, Boros LG, Nissen N, Heaney AP. Fructose induces transketolase flux to promote pancreatic cancer growth. Cancer Res. 2010;70:6368–6376. [PubMed: 20647326]
167. Keshari KR, Wilson DM, Chen AP, et al. Hyperpolarized [2-^{13}C]-fructose: a hemiketal DNP substrate for *in vivo* metabolic imaging. J Am Chem Soc. 2009;131:17591–17596. [PubMed: 19860409]
168. Park JM, Wu M, Datta K, et al. Hyperpolarized sodium [1-^{13}C]-glycerate as a probe for assessing glycolysis *in vivo*. J Am Chem Soc. 2017;139:6629–6634. [PubMed: 28467066]
169. Stincone A, Prigione A, Cramer T, et al. The return of metabolism: biochemistry and physiology of the pentose phosphate pathway. Biol Rev. 2015;90:927–963. [PubMed: 25243985]
170. Jiang P, Du W, Wu M. Regulation of the pentose phosphate pathway in cancer. Protein Cell. 2014;5:592–602. [PubMed: 25015087]
171. Timm KN, Hartl J, Keller MA, et al. Hyperpolarized [U-^{2}H, U-^{13}C] glucose reports on glycolytic and pentose phosphate pathway activity in EL4 tumors and glycolytic activity in yeast cells. Magn Reson Med. 2015;74:1543–1547. [PubMed: 25522215]
172. Moreno KX, Harrison CE, Merritt ME, Kovacs Z, Malloy CR, Dean SA. Hyperpolarized δ-[1–13C] gluconolactone as a probe of the pentose phosphate pathway. NMR Biomed. 2017;30:e3713.
173. Leder IG. Hog kidney gluconokinase. J Biol Chem. 1957;225:125–136. [PubMed: 13416223]
174. Rohatgi N, Guðmundsson S, Rolfsson Ó. Kinetic analysis of gluconate phosphorylation by human gluconokinase using isothermal titration calorimetry. FEBS Lett. 2015;589:3548–3555. [PubMed: 26505675]
175. Schafer FQ, Buettner GR. Redox environment of the cell as viewed through the redox state of the glutathione disulfide/glutathione couple. Free Radic Biol Med. 2001;30:1191–1212. [PubMed: 11368918]
176. Timm KN, Hu D-E, Williams M, et al. Assessing oxidative stress in tumors by measuring the rate of hyperpolarized [1-^{13}C] dehydroascorbic acid reduction using ^{13}C magnetic resonance spectroscopy. J Biol Chem. 2017;292:1737–1748. [PubMed: 27994059]
177. Vander Heiden MG, DeBerardinis RJ. Understanding the intersections between metabolism and cancer biology. Cell. 2017;168:657–669. [PubMed: 28187287]

178. Kang YP, Ward NP, DeNicola GM. Recent advances in cancer metabolism: a technological perspective. Exp Mol Med. 2018;50:31. [PubMed: 29657324]

179. Taegtmeyer H Cardiac metabolism as a target for the treatment of heart failure. Circulation. 2004;110:894–896. [PubMed: 15326079]

180. Martinez-Outschoorn UE, Peiris-Pagés M, Pestell RG, Sotgia F, Lisanti MP. Cancer metabolism: a therapeutic perspective. Nat Rev Clin Oncol. 2016;14:11–31. [PubMed: 27141887]

181. McLaughlin T, Abbasi F, Cheal K, Chu J, Lamendola C, Reaven G. Use of metabolic markers to identify overweight individuals who are insulin resistant. Ann Intern Med. 2003;139:802–809. [PubMed: 14623617]

182. Aggarwal R, Vigneron DB, Kurhanewicz J. Hyperpolarized 1-[^{13}C]-pyruvate magnetic resonance imaging detects an early metabolic response to androgen ablation therapy in prostate cancer. Eur Urol. 2017;72:1028–1029. [PubMed: 28765011]

183. Nelson SJ, Kurhanewicz J, Vigneron DB, et al. Metabolic imaging of patients with prostate cancer using hyperpolarized [1-^{13}C]pyruvate. Sci Transl Med. 2013;5:198ra108.

184. Park I, Larson Peder EZ, Gordon JW, et al. Development of methods and feasibility of using hyperpolarized carbon-13 imaging data for evaluating brain metabolism in patient studies. Magn Reson Med. 2018;80:864–873. [PubMed: 29322616]

185. Miloushev VZ, Granlund KL, Boltyanskiy R, et al. Metabolic imaging of the human brain with hyperpolarized ^{13}C pyruvate demonstrates ^{13}C lactate production in brain tumor patients. Cancer Res. 2018;78:3755–3760. [PubMed: 29769199]

186. Randle PJ, Garland PB, Hales CN, Newsholme EA. The glucose fatty-acid cycle its role in insulin sensitivity and the metabolic disturbances of diabetes mellitus. Lancet. 1963;281:785–789.

187. Opie LH. Chapter 2—Cardiac metabolism in health and disease In: Willis MS, Homeister JW, Stone JR, eds. Cellular and Molecular Pathobiology of Cardiovascular Disease. San Diego, CA: Academic; 2014:23–36.

188. Ardenkjaer-Larsen JH, Leach AM, Clarke N, Urbahn J, Anderson D, Skloss TW. Dynamic nuclear polarization polarizer for sterile use intent. NMR Biomed. 2011;24:927–932. [PubMed: 21416540]

189. Gajan D, Bornet A, Vuichoud B, et al. Hybrid polarizing solids for pure hyperpolarized liquids through dissolution dynamic nuclear polarization. ProcNatl Acad Sci U S A. 2014;111:14693–14697.

190. Baudouin D, van Kalkeren HA, Bornet A, et al. Cubic three-dimensional hybrid silica solids for nuclear hyperpolarization. Chem Sci. 2016;7:6846–6850. [PubMed: 28451127]

191. Zhang Y, Baker PJ, Casabianca LB. BDPA-doped polystyrene beads as polarization agents for DNP-NMR. J Phys Chem B. 2016;120:18–24. [PubMed: 26717243]

192. Dollmann BC, Junk MJN, Drechsler M, Spiess HW, Hinderberger D, Münnemann K. Thermoresponsive, spin-labeled hydrogels as separable DNP polarizing agents. Phys Chem Chem Phys. 2010;12:5879–5882. [PubMed: 20518113]

193. Eichhorn TR, Takado Y, Salameh N, et al. Hyperpolarization without persistent radicals for *in vivo* real-time metabolic imaging. Proc Natl Acad Sci U S A. 2013;110:18064–18069. [PubMed: 24145405]

194. Taglang C, Korenchan DE, von Morze C, et al. Late-stage deuteration of ^{13}C-enriched substrates for T_1 prolongation in hyperpolarized ^{13}C MRI. Chem Commun. 2018;54:5233–5236.

195. Niedbalski P, Wang Q, Parish C, Khashami F, Kiswandhi A, Lumata L. Magnetic-field-dependent lifetimes of hyperpolarized ^{13}C spins at cryogenic temperature. J Phys Chem B. 2018;122:1898–1904. [PubMed: 29369632]

196. Niedbalski P, Parish C, Kiswandhi A, Kovacs Z, Lumata L. Influence of ^{13}C isotopic labeling location on dynamic nuclear polarization of acetate. J Phys Chem A. 2017;121:3227–3233. [PubMed: 28422500]

197. Ji X, Bornet A, Vuichoud B, et al. Transportable hyperpolarized metabolites. Nat Commun. 2017;8:13975. [PubMed: 28072398]

198. Capozzi A, Cheng T, Boero G, Roussel C, Comment A. Thermal annihilation of photo-induced radicals following dynamic nuclear polarization to produce transportable frozen hyperpolarized ^{13}C-substrates. Nat Commun. 2017;8:15757. [PubMed: 28569840]

199. Carravetta M, Levitt MH. Long-lived nuclear spin states in high-field solution NMR. J Am Chem Soc. 2004;126:6228–6229. [PubMed: 15149209]

200. Carravetta M, Levitt MH. Theory of long-lived nuclear spin states in solution nuclear magnetic resonance. I. Singlet states in low magnetic field. J Phys Chem. 2005;122:214505.

201. Marco-Rius I, Tayler MCD, Kettunen MI, et al. Hyperpolarized singlet lifetimes of pyruvate in human blood and in the mouse. NMR Biomed. 2013;26:1696–1704. [PubMed: 23946252]

202. Pileio G, Carravetta M, Levitt MH. Storage of nuclear magnetization as long-lived singlet order in low magnetic field. Proc Natl Acad Sci U S A. 2010;107:17135–17139. [PubMed: 20855584]

203. Feng Y, Theis T, Liang X, Wang Q, Zhou P, Warren WS. Storage of hydrogen spin polarization in long-lived ^{13}C2 singlet order and implications for hyperpolarized magnetic resonance imaging. J Am Chem Soc. 2013;135:9632–9635. [PubMed: 23781874]

204. Warren WS, Jenista E, Branca RT, Chen X. Increasing hyperpolarized spin lifetimes through true singlet eigenstates. Science. 2009;323:1711. [PubMed: 19325112]

205. Levitt MH. Singlet nuclear magnetic resonance. Annu Rev Phys Chem. 2012;63:89–105. [PubMed: 22224703]

206. Sarkar R, Vasos PR, Bodenhausen G. Singlet-state exchange NMR spectroscopy for the study of very slow dynamic processes. J Am Chem Soc. 2007;129:328–334. [PubMed: 17212412]

207. Hurd RE, Yen Y-F, Mayer D, et al. Metabolic imaging in the anesthetized rat brain using hyperpolarized [1-^{13}C] pyruvate and [1-^{13}C] ethyl pyruvate. Magn Reson Med. 2010;63:1137–1143. [PubMed: 20432284]

208. Billingsley KL, Josan S, Park JM, et al. Hyperpolarized [1,4-^{13}C]-diethylsuccinate: a potential DNP substrate for *in vivo* metabolic imaging. NMR Biomed. 2014;27:356–362. [PubMed: 24421249]

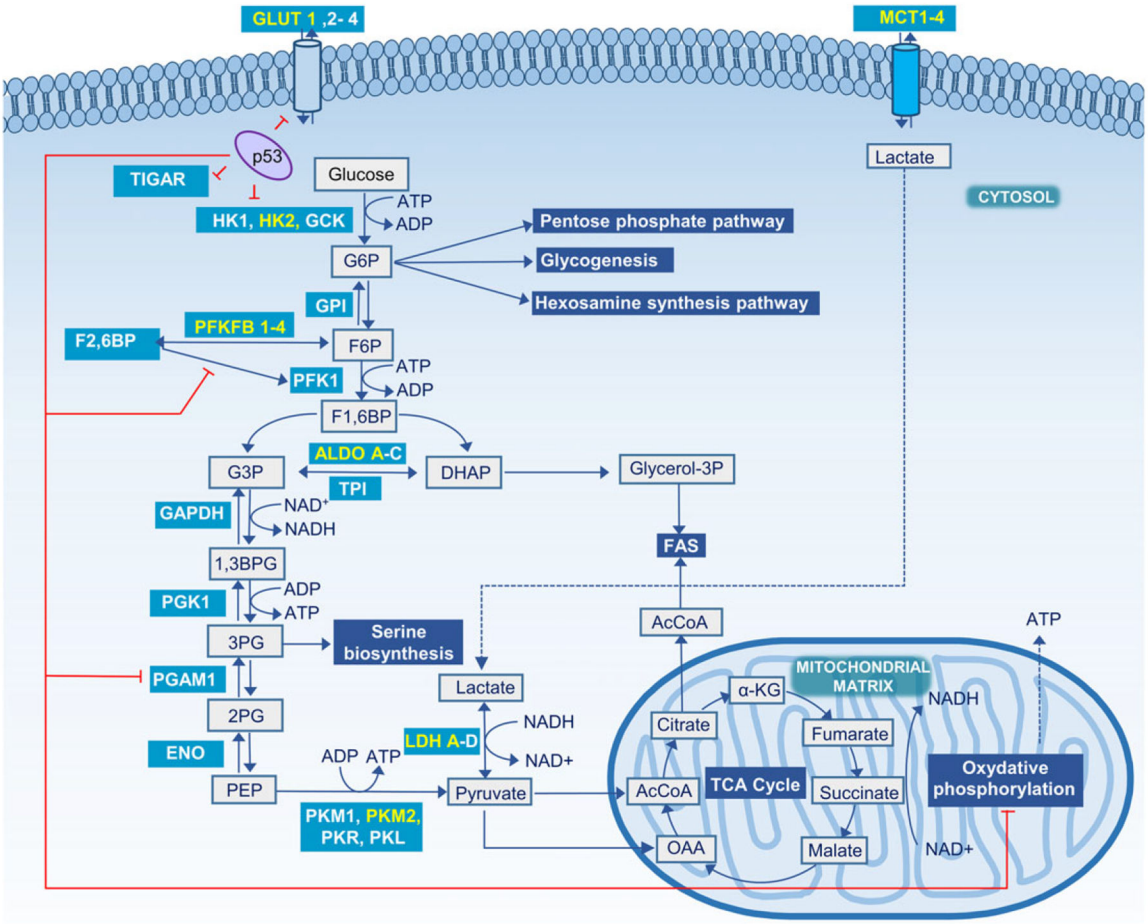

FIGURE 1.

Glycolysis and major steps in glucose metabolism. Metabolic reactions are shown in grey boxes, glycolysis associated pathways in blue-shaded boxes, and enzymes in teal-shaded boxes with those predominant in cancer cells highlighted in yellow. Sites regulated by the tumor suppressor protein *p53* are indicated with red lines. 1,3BPG, 1,3-bisphosphoglycerate; 2PG, 2-phosphoglycerate; 3PG, 3-phosphoglycerate; α-KG, α-ketoglutarate; AcCoA, acetyl-CoA; ALDO, aldolase; DHAcP, dihydroxyacetone phosphate; ENO, enolase; F1,6BP, fructose 1,6-bisphosphate; F2,6BP, fructose 2,6-bisphosphate; F6P, fructose 6-phosphate; FAS, fatty acid synthase; G6P, glucose 6-phosphate; GAPDH, glyceraldehyde-3-phosphate dehydrogenase; GCK, glucokinase; GLUT, glucose transporter; glycerol-3P, glycerol 3-phosphate; GPI, glucose 6-phosphate isomerase; HK, hexokinase; OAA, oxaloacetate; *p53*, cellular tumor antigen *TP53*; PFK1, phosphofructokinase 1; PFKFB, 6-phosphofructo-2-kinase/fructose-2,6-bisphosphatase; PGAM1, phosphoglycerate mutase 1; PGK1, phosphoglycerate kinase 1; PK, pyruvate kinase; TPI, triosephosphate isomerase

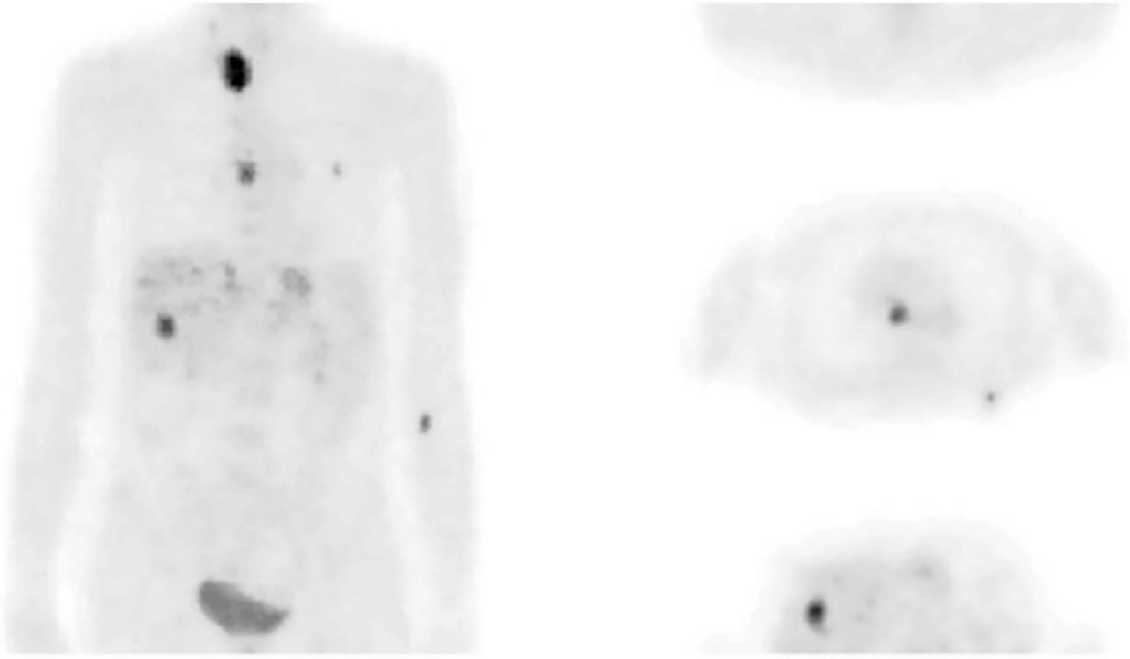

FIGURE 2.

An example of ^{18}F-FDG-PET. A whole-body ^{18}F-FDG study of a patient with metastases from colon cancer (left, projection; right, three representative transaxial slices). The PET scan began 40 min after injection of 370 MBq of ^{18}F-FDG. (Reproduced with permission from Reference 41)

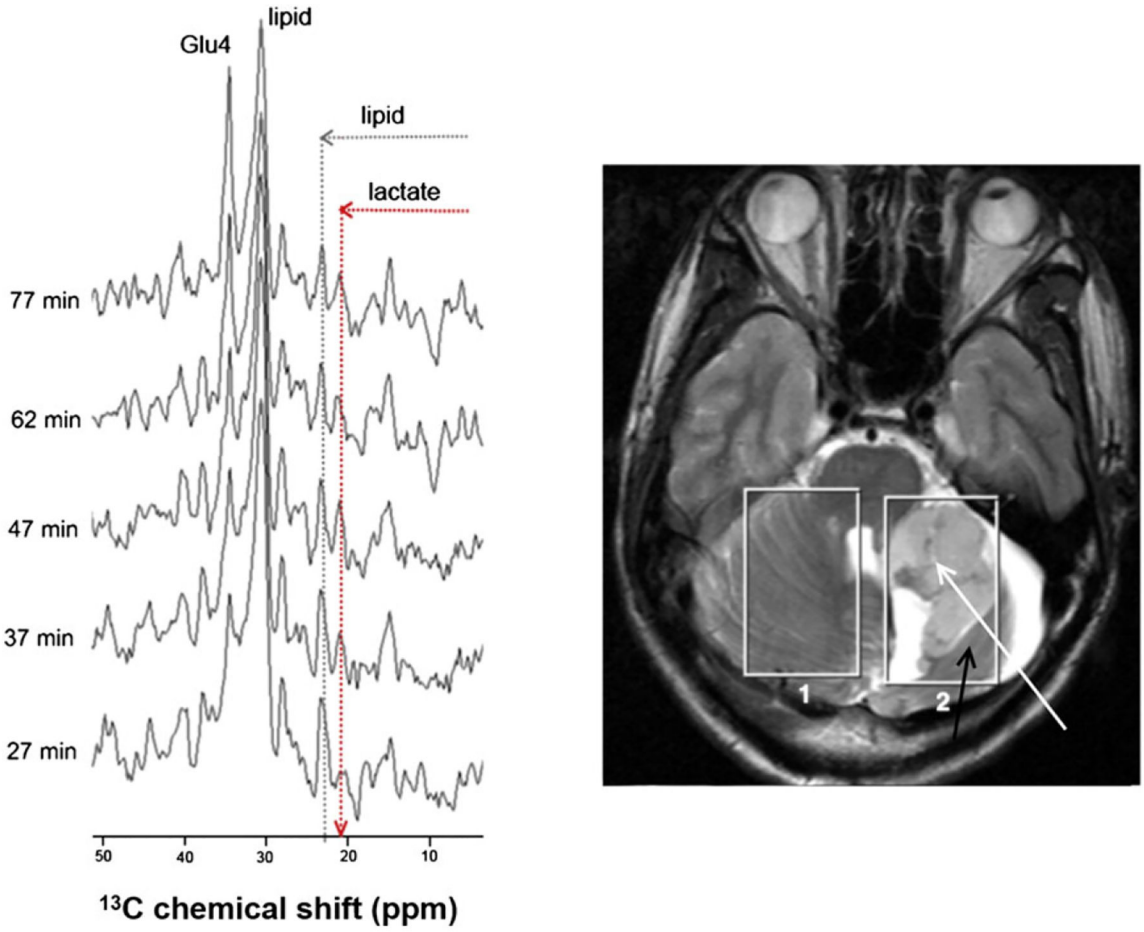

FIGURE 3.

^{13}C MR spectra of the tumor region of a patient with high grade glioma after administration of [1-^{13}C]-D-glucose (left). The ^{1}H MR images (right) show the position of the two voxels (size 50 cm^{3}) used for the ^{13}C MRS. Voxel 1 is positioned in healthy cerebellum while Voxel 2 covers the tumor (white arrow) as well as some normal brain tissue (black arrow). The hyperintense areas are fluid filled. (Reproduced with permission from Reference 59)

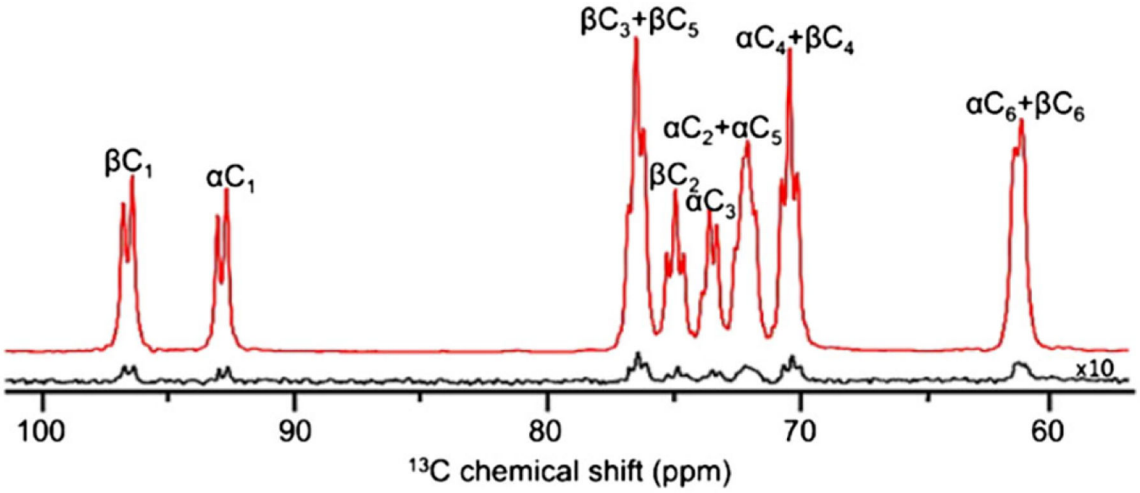

FIGURE 4.

^{2}H decoupled ^{13}C DNP NMR spectrum of hyperpolarized [U-$^{13}C_6$, U-$^{2}H_7$]- D-glucose in D_2O at 9.4 T. The hyperpolarized spectrum (red) was recorded using a single scan with a 9° flip angle while the thermally polarized spectrum was acquired in 16 scans with a 45° flip angle after the decay of hyperpolarized magnetization. The spectra show the ^{13}C carbons of the α and β anomers as multiplets due to ^{13}C homonuclear J_{12} couplings. (Reproduced with permission from Reference 62)

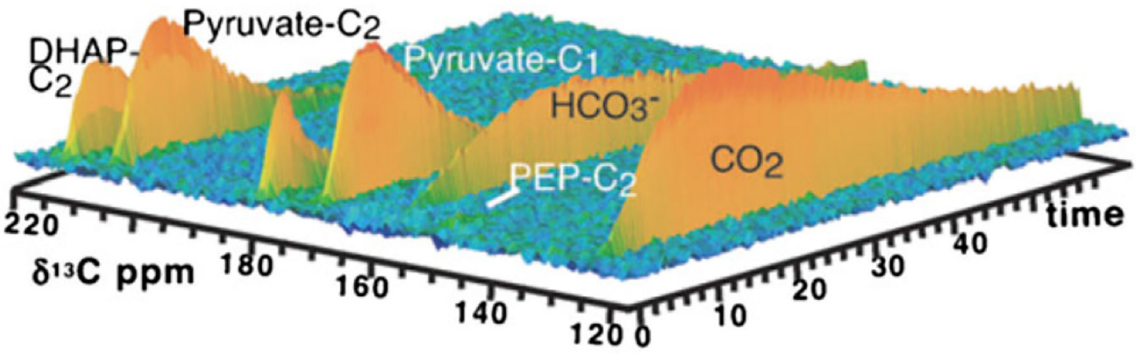

FIGURE 5.

Time evolution of the carbonyl ^{13}C signals of metabolites observed in cell suspensions of *S. cerevisiae* fed with 4 mM hyperpolarized [U-$^{13}C_6$, U-$^{2}H_7$]-D-glucose. The spectra were recorded using a 6° flip angle with 500 ms temporal resolution at 14.1 T and 30 °C. The aliphatic region is not shown. (Reproduced with permission from Reference 61)

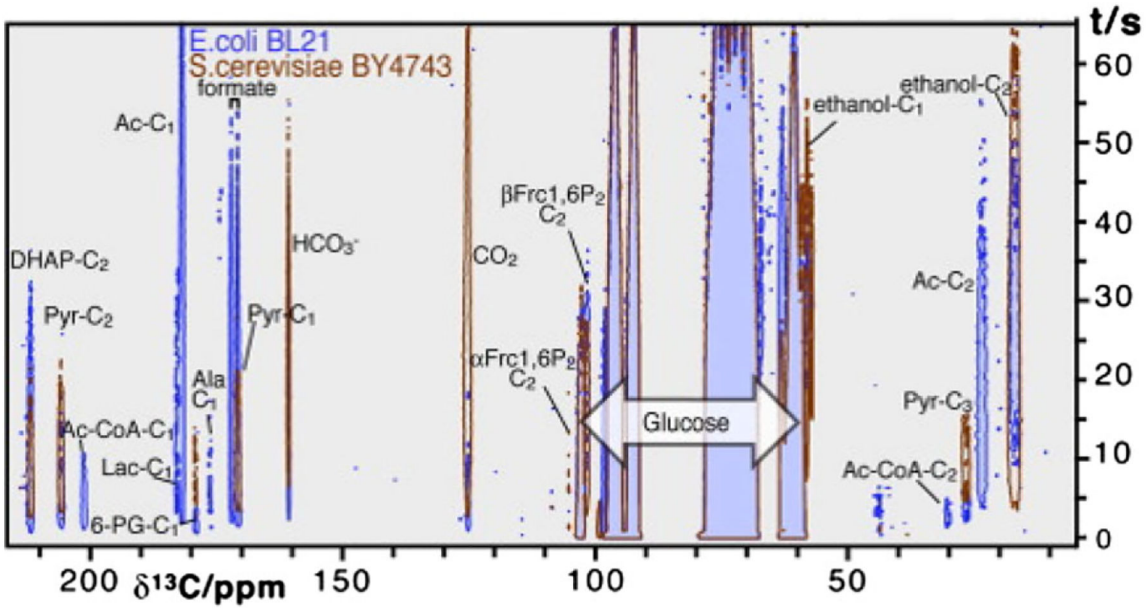

FIGURE 6.

Time evolution of the ^{13}C signals of various metabolites of hyperpolarized [U-$^{13}C_6$, U-$^{2}H_7$]-D-glucose in *S. cerevisiae* and *E. coli*. (Reproduced with permission from Reference 60)

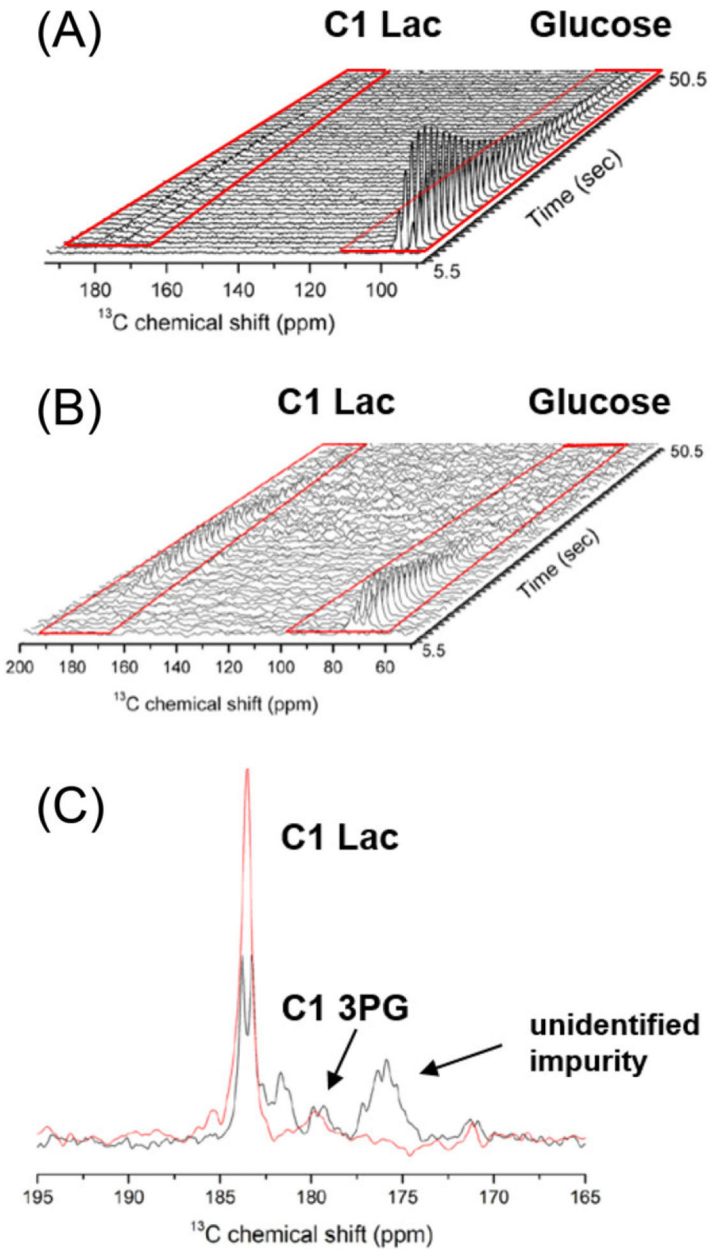

FIGURE 7.

A, B, Metabolism of hyperpolarized [U-$^{13}C_6$, U-$^{2}H_7$]-D-glucose (A) and hyperpolarized [3,4-$^{13}C_2$, 2,3,4,6,6-$^{2}H_5$]-D-glucose (B) in the mouse brain. C, The ^{13}C signal of C1 lactate appeared as a doublet when [U-$^{13}C_6$, U-$^{2}H_7$]-D-glucose was used (black) and as a more intense singlet when [3,4-$^{13}C_2$, 2,3,4,6,6-$^{2}H_5$]-D-glucose was used (red). (Reproduced with permission from Reference 103)

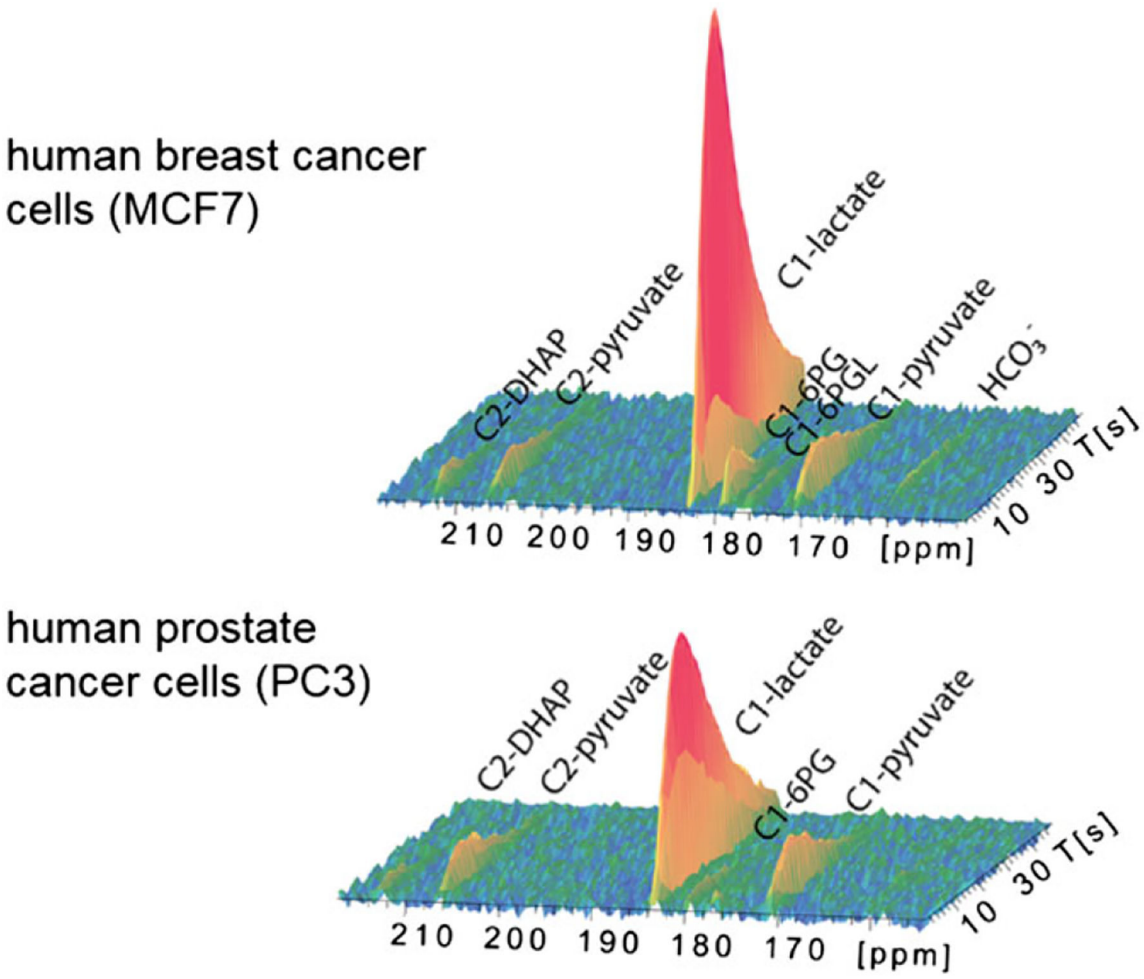

FIGURE 8.

Metabolism of hyperpolarized [U-$^{13}C_6$, U-$^{2}H_7$]-D-glucose in MCF7 human breast cancer cells and PC3 human prostate cancer cell over 50 s with a 2 s time resolution. The observed signals were assigned to the C2 of DHAcP (212.6 ppm), C2 of pyruvate (206 ppm), C1 of lactate (183.5 ppm), C1 of 6-phosphogluconate (179.8 ppm), C1 of 6-phosphogluconolactone (177 ppm), C1 of pyruvate (171.6 ppm) and bicarbonate (161.4 ppm). (Reproduced with permission from Reference 122)

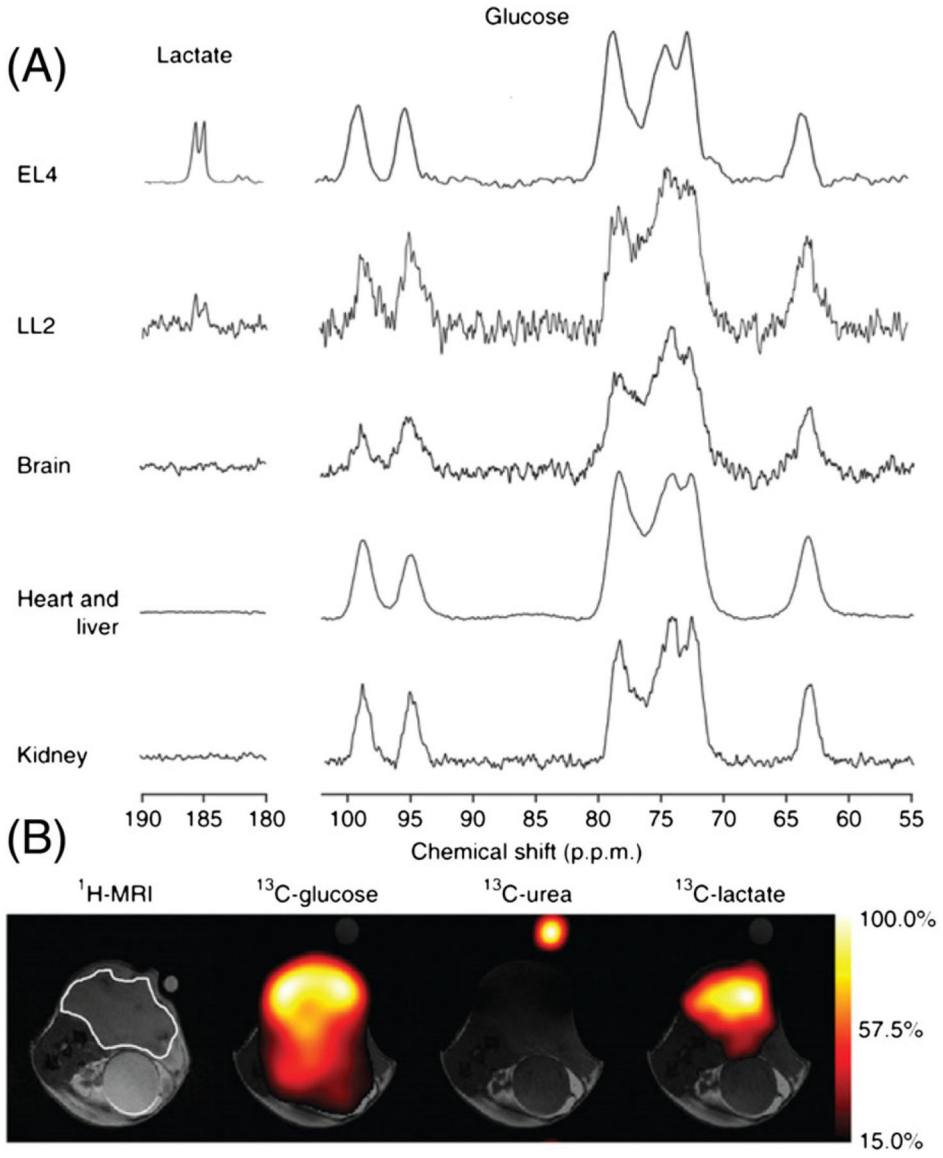

FIGURE 9.

A, Representative ^{13}C MR spectra recorded at 7 T in subcutaneous EL4 and LL2 tumors, normal brain, heart and liver, and kidneys 15 s after injection of hyperpolarized [U-$^{13}C_6$, U-$^{2}H_7$]-D-glucose (350 μL, 100 mM) into a tumor bearing mouse. B, Representative ^{13}C chemical shift images recorded 15 s after i.v. injection of hyperpolarized [U-$^{13}C_6$, U-$^{2}H_7$]-D-glucose (400 μL, 200 mM) into an EL4 tumor bearing mouse. The location of the tumor is marked in white in the ^{1}H MR image. (Reproduced with permission from Reference 63)

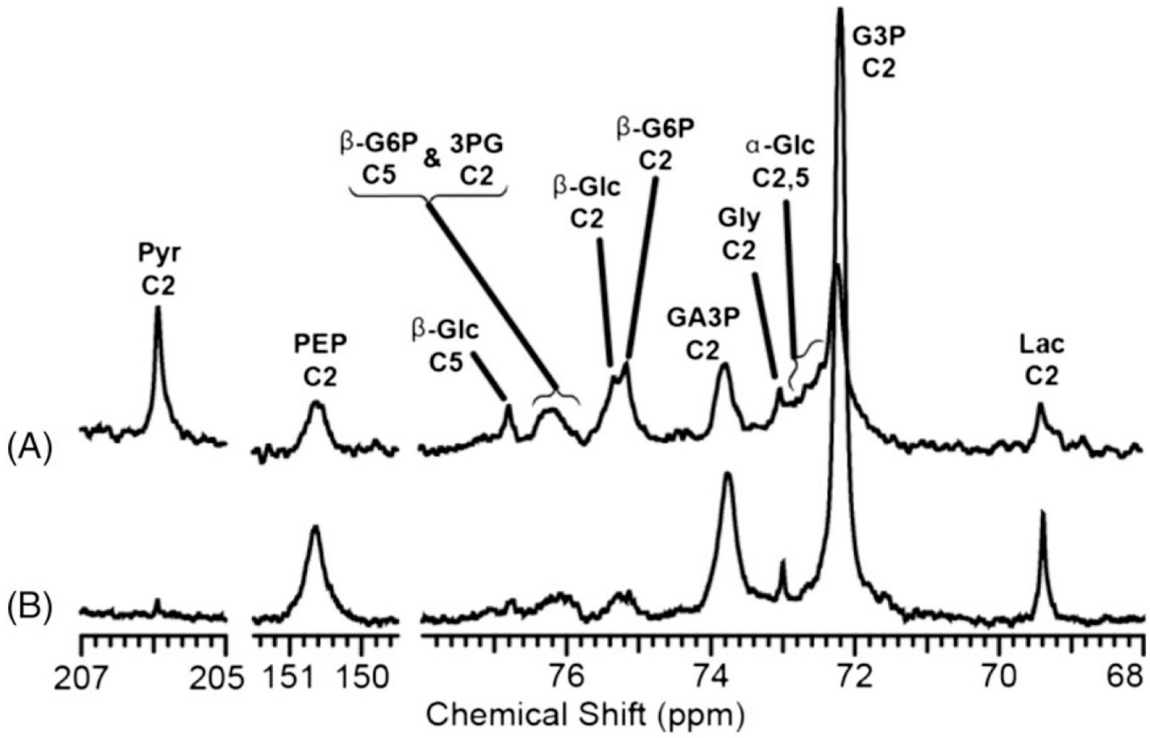

FIGURE 10.

Various upstream and downstream metabolites of hyperpolarized [2-^{13}C] DHAc detected by ^{13}C NMR at 9.4 T in isolated, perfused mouse livers in gluconeogenic A, versus glycogenolytic state B,. The spectra represent a sum of 35 scans (3 s repetition time) acquired with 30° pulses after the injection of hyperpolarized [2-^{13}C] DHAc. (Reproduced with permission from Reference 125)

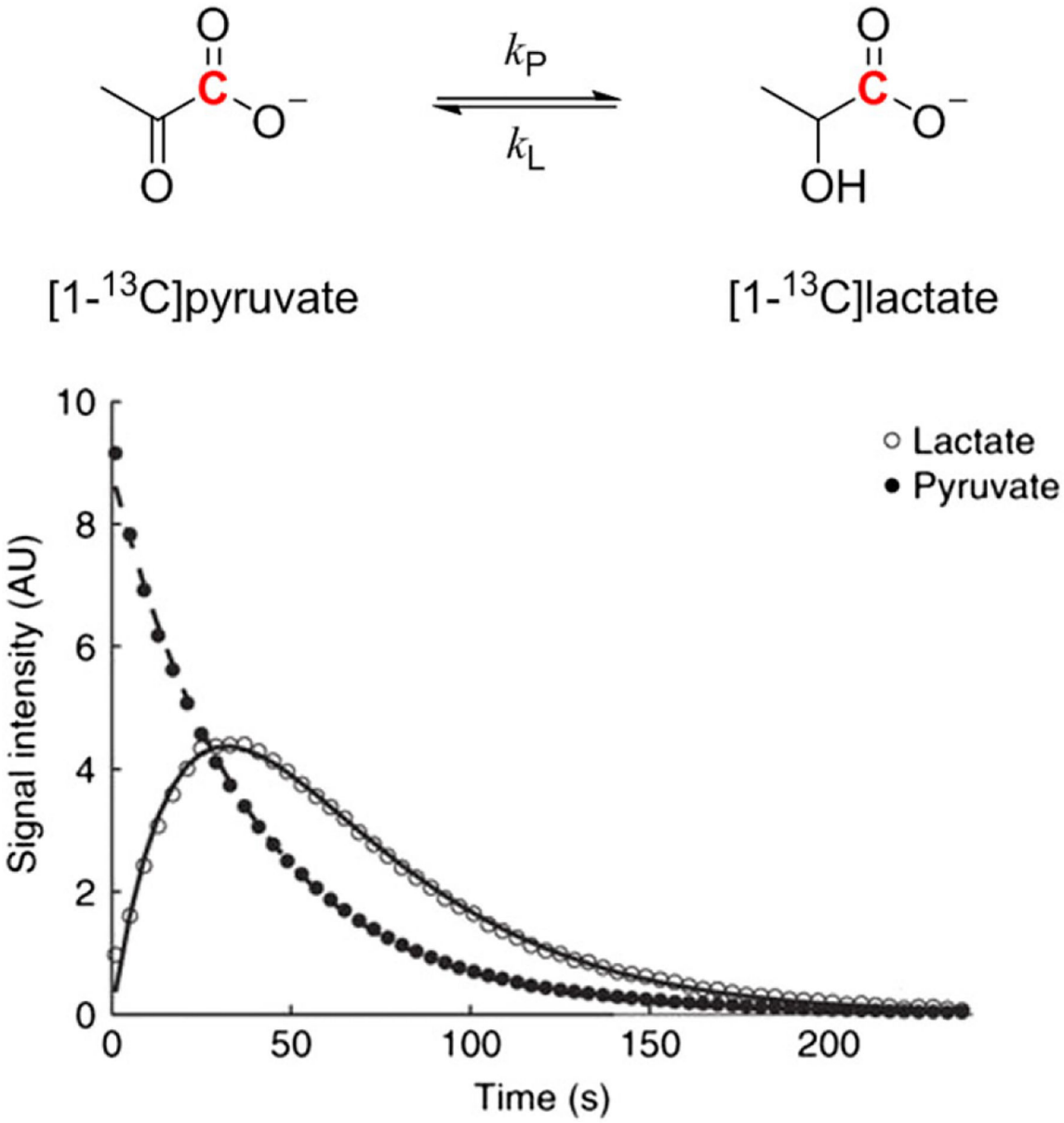

FIGURE 11.

The hyperpolarized ^{13}C label in [1-^{13}C] pyruvate rapidly exchanges into a preexisting lactate pool. The C1 ^{13}C signal of lactate first increases as the label is transferred from pyruvate and then decreases due to T_1 decay of the hyperpolarized magnetization. The k_P and k_L rate constants as well as the T_1 values can be calculated by fitting the C1 ^{13}C signal intensities of pyruvate and lactate to the modified Bloch equations written for a two-site exchange. (Reproduced with permission from Reference 148)

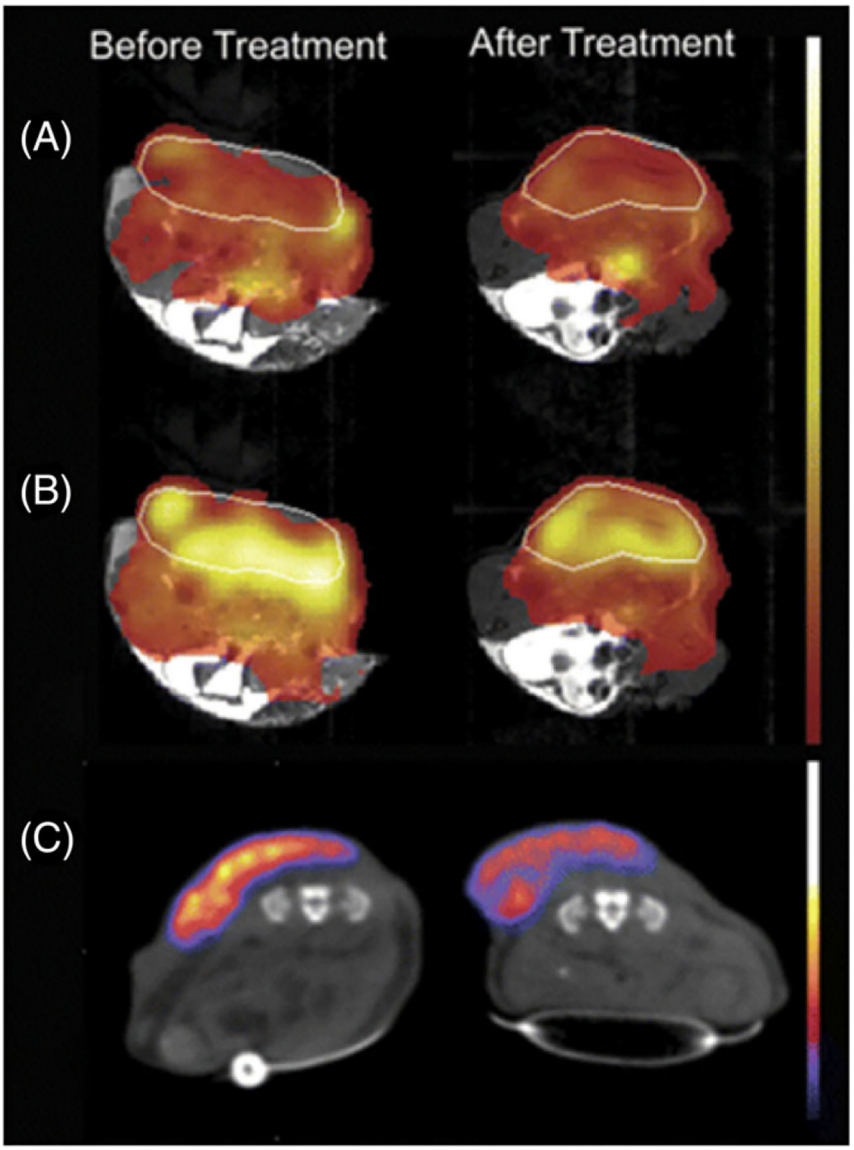

FIGURE 12.

Comparison of [1-^{13}C] pyruvate DNP-MRS and ^{18}F-FDG PET in a murine lymphoma model. The tumor margins are marked with a white line. A, Spatial distribution of injected hyperpolarized [1-^{13}C] pyruvate before and 24 h after treatment with etoposide. The MR images were acquired from the same animal. Normalized ^{13}C chemical shift images of [1-^{13}C] pyruvate distribution are overlaid on gray-scale ^{1}H MR images. B, Spatial distribution of hyperpolarized [1-^{13}C] lactate after the injection of hyperpolarized [1-^{13}C]pyruvate. C, PET images acquired between 80 and 90 min after injection of 7 MBq of ^{18}F-FDG. Images were acquired before and after treatment, and the PET images have been overlaid on gray-scale CT images. The MRI and PET experiments were performed using different animals. (Reproduced with permission from Reference 143)

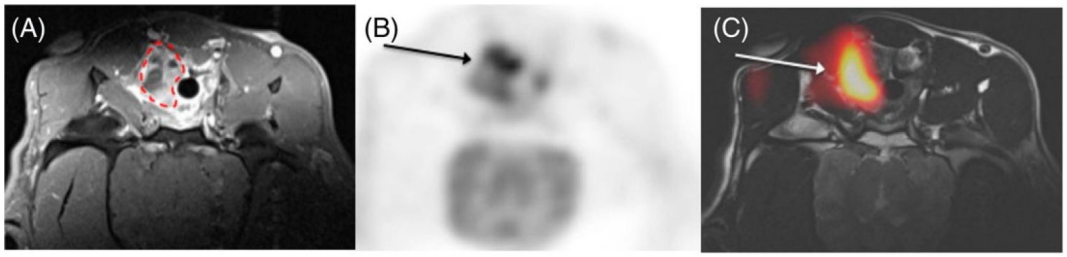

FIGURE 13.

A, T_1-weighted, Gd-enhanced ^{1}H MR image of a canine neck squamous cell carcinoma tumor, marked with a red line. B, C, ^{18}F-FDG-PET image shows variable ^{18}F-FDG uptake in the tumor (B) that does not correspond to regions of high lactate production seen in the ^{13}C MR image (C). (Reproduced with permission from Reference 154)

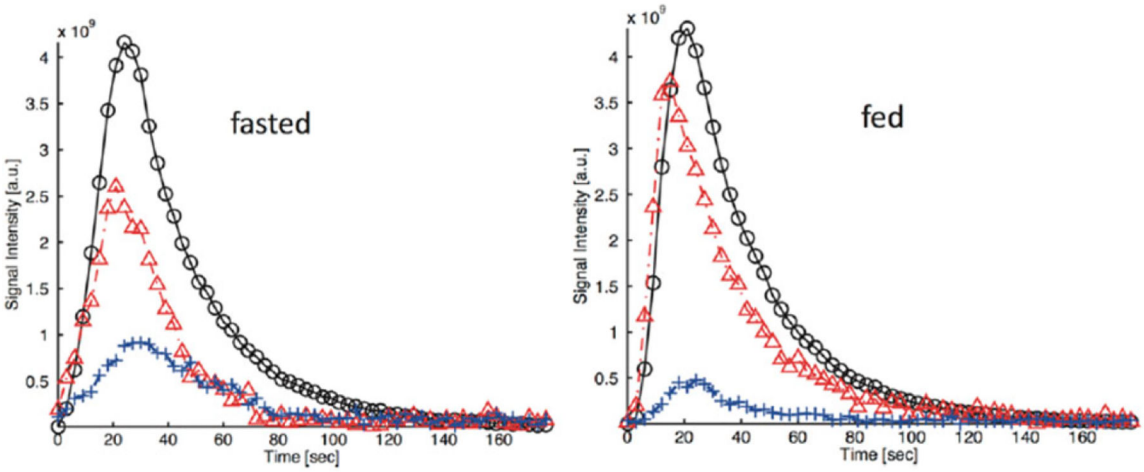

FIGURE 14.

Time evolution of the hyperpolarized signal of [1-^{13}C] glycerate (○), [1-^{13}C] lactate (△) and [1-^{13}C] pyruvate (+) in the liver of fasted and fed rats injected with hyperpolarized [1-^{13}C] glycerate (1 mmol/kg dose). The data were collected at 3 T with a custom-built ^{13}C transmit/receive surface coil (diameter = 28 mm) placed over the liver. (Reproduced with permission from Reference 168)

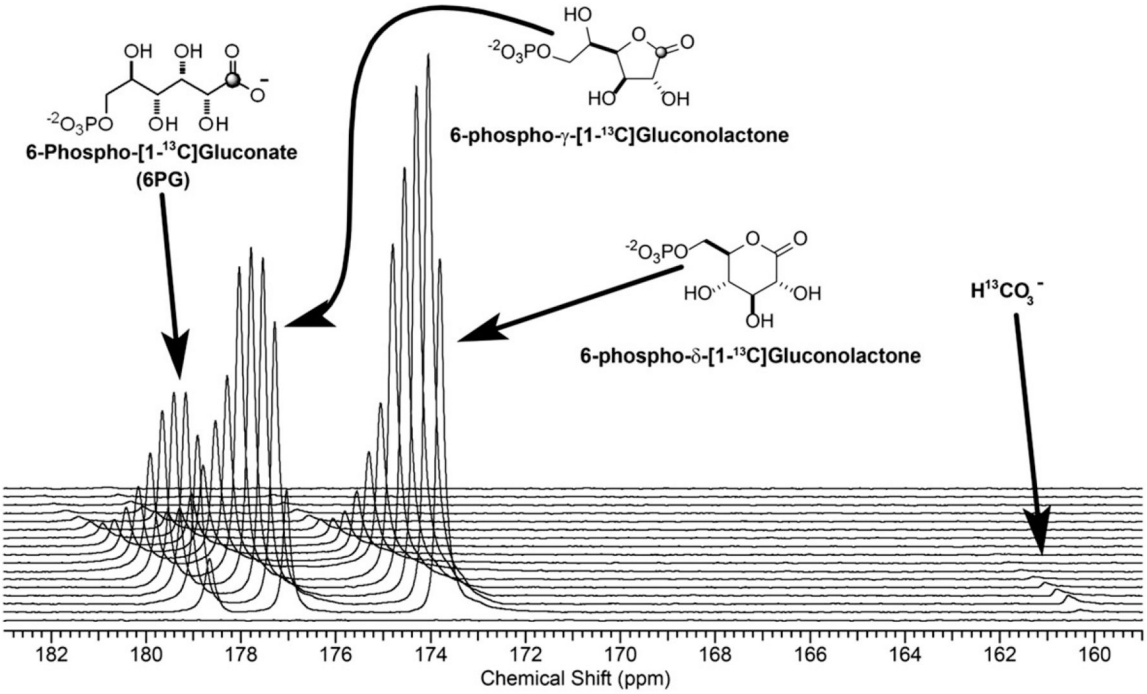

FIGURE 15.

A plot of ^{13}C NMR spectra collected on an isolated mouse liver after perfusion with hyperpolarized [1-^{13}C]-D-glucono-δ-lactone (4 mM) and octanoate (0.4 mM). The ^{13}C spectra were collected every 5 s using a 66° pulse at 9.4 T. (Reproduced with permission from Reference 172)

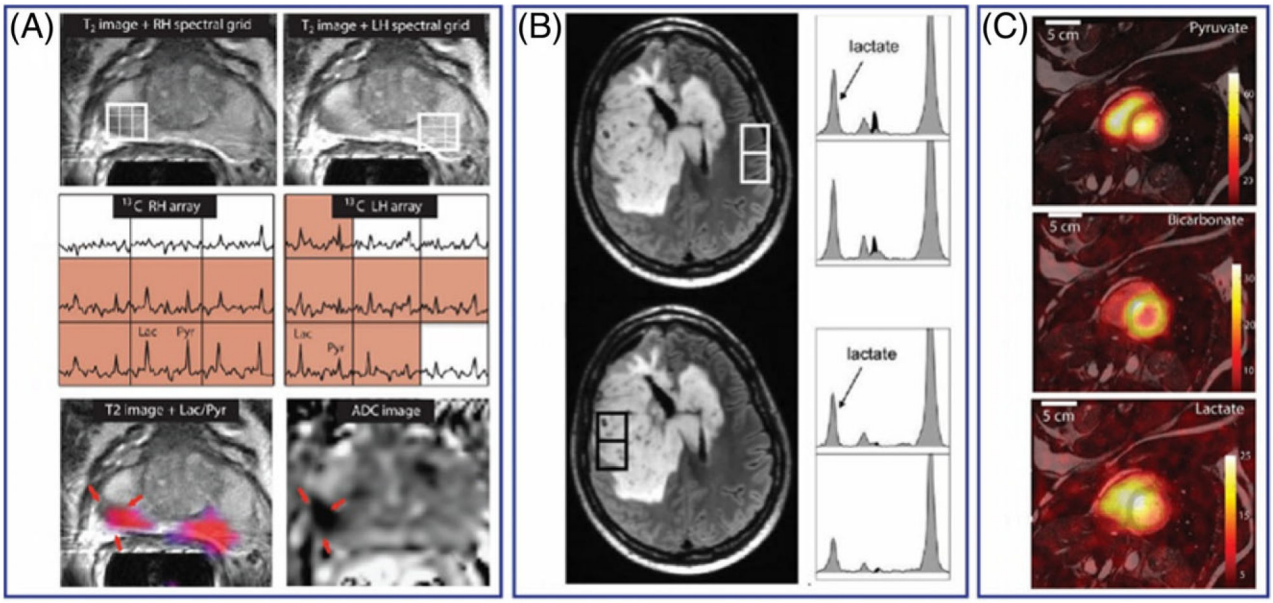

FIGURE 16.

A, Hyperpolarized ^{13}C MRSI of a prostate tumor in a human patient. The top images show the T_2-weighted MRI of the prostate. ^{13}C spectra arrays of the voxels indicated in the above ^{1}H image show intense lactate signal in the tumor areas. ^{13}C lactate/pyruvate ratio maps overlaid on a ^{1}H image and an ADC (apparent diffusion coefficient) image are shown in the bottom panel. B, Hyperpolarized ^{13}C MRSI of a patient with brain tumor showing the lactate peaks in a tumor and normal appearing brain regions. C, Hyperpolarized^{13}C signal intensity maps of [1-^{13}C] pyruvate, [^{13}C] bicarbonate, and [1-^{13}C] lactate of the heart from a healthy volunteer. Adapted from References 136, 183, 184, and with permission

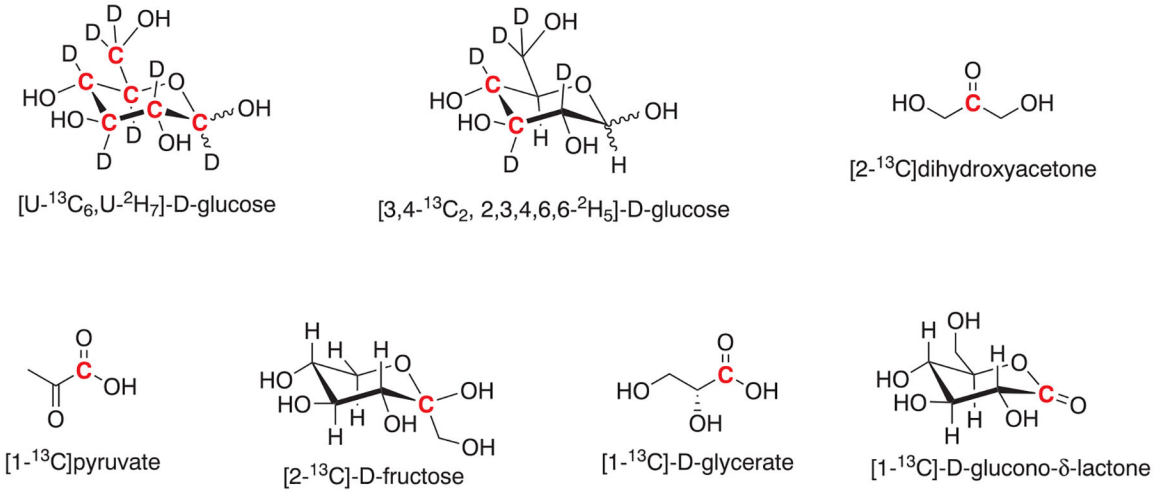

CHART 1.

^{13}C-labeled metabolic probes used to monitor glycolysis by hyperpolarized ^{13}C MRS/MRI. The position of the ^{13}C label is highlighted in red